

This manuscript has undergone peer-review and has been accepted for publication in the journal *Marine and Petroleum Geology*. This manuscript has not undergone typesetting by the publisher. An updated peer-reviewed publication DOI link will be included when it becomes available.

1 Kinematic interaction between stratigraphically discrete salt 2 layers; the structural evolution of the Corrib gas field, offshore 3 NW Ireland

4 Conor O'Sullivan^{1,2}, Conrad Childs^{1,2}

5 ¹ Irish Centre for Research in Applied Geoscience (iCRAG), School of Earth Sciences, University College Dublin,
6 Belfield, Dublin 4, Ireland

7 ² Fault Analysis Group, School of Earth Sciences, University College Dublin, Belfield, Dublin 4, Ireland

8 Corresponding author email: conor.osullivan@icrag-centre.org

9 Abstract

10 The kinematic interaction of thin salt layers during basin evolution has received little attention
11 to date, despite there being several basins which contain multiple thin salt layers across NW
12 Europe. This study utilises high-quality 3D seismic reflection data coupled with borehole data
13 to investigate the evolution of the structure containing the Corrib gas field which is composed
14 of two distinct salt structures. Located in the Slyne Basin offshore NW Ireland, the structure
15 consists of a NE-SW oriented Permian salt anticline which folds the overlying Mesozoic
16 stratigraphy. Upper Triassic salt acts as a second mechanical detachment and forms an
17 elongate salt roller parallel to the crest of the Permian salt anticline. The Upper Triassic salt
18 roller forms the footwall of a listric fault which downthrows the anticlinal crest of the folded
19 Jurassic section to the SE. The Permian salt anticline began rising during the Late Triassic
20 and Early Jurassic driven by low-strain regional extension. During the main phase of rifting, a
21 combination of basement tilting, gravity gliding, and salt welding resulted in a steep increase
22 in the amplitude of the Permian salt anticline. The relief on the salt-cored fold resulted in gravity
23 gliding on the Triassic salt, forming the parallel salt roller and listric fault. The throw distribution
24 on the listric fault is driven by the combined mechanisms of gravity sliding on the Triassic salt
25 and by inflation of Triassic salt in the footwall of the fault. The listric fault is reactivated post-
26 rift, suggesting modification of the Permian and Triassic salt structures. This study improves
27 the understanding of the kinematic interaction of thin salt layers during syn-rift and post-rift
28 deformation, with implications for hydrocarbon exploration on the Irish Atlantic margin and
29 further afield.

30 Acknowledgements

31 This research is funded in part by a research grant from Science Foundation Ireland (SFI)
32 under Grant Number 13/RC/2092 and is co-funded under the European Regional

33 Development Fund, and by the Petroleum Infrastructure Programme (PIP) and its member
34 companies. The authors thank reviewers Katherine A. Giles and Davide Gamboa for their
35 constructive reviews which greatly improved the manuscript. The authors thank the Petroleum
36 Affairs Division (PAD) of the Department of Communications, Climate Action and Environment
37 (DCCA), Ireland, for providing access to released well and seismic reflection datasets. Shell
38 Exploration & Production Ireland Ltd. are thanked for providing access to reprocessed
39 volumes of the 1997 Corrib seismic. Europa Oil & Gas are thanked for providing access to the
40 Inishkea 2018 reprocessed seismic volume and allowing a section from the volume to be
41 shown. The authors thank Schlumberger for providing academic licenses of Petrel to
42 University College Dublin. The authors also thank Petroleum Experts for providing academic
43 licenses of Move to University College Dublin.

44 Introduction

45 The presence of salt layers in the stratigraphy of a basin influences structural style both by
46 mechanically detaching sub- and supra-salt stratigraphy during extension or compression, and
47 by halokinesis to form salt pillows and diapirs (Jackson & Talbot, 1991; Stewart et al., 1996;
48 Withjack & Callaway, 2000; Hudec & Jackson, 2007; Duffy et al., 2013). As salt moves from
49 its original stratigraphic position it can also form allochthonous salt structures such as pinched
50 diapirs and canopies. Where large salt canopies develop, they will act as a second layer of
51 mechanical detachment and different structures can form above and below these
52 allochthonous salt bodies. This also opens the possibility of kinematic interaction between
53 primary and secondary halokinetic structures in the autochthonous and allochthonous salt
54 layers (Volozh et al., 2003; Jackson et al., 2010; Dooley et al., 2013; Dooley et al., 2018). The
55 resulting wide variety of salt-related structures has been observed and investigated in several
56 salt-prone basins around the world, including offshore Iberia (Wilson et al., 1989; Ferrer et al.,
57 2012; Ramos et al., 2017), the Gulf of Mexico (Peel et al., 1995; Dooley et al., 2013), the
58 Canadian Atlantic margin (Deptuck & Kendell, 2017) and several basins along both the
59 Brazilian and West African Atlantic margins (Tari et al., 2003; Davison, 2007).

60 There are comparatively few studies of the interaction between multiple autochthonous salt
61 layers. In the Persian Gulf, Cambrian and Cenozoic salt layers, separated by several
62 kilometres of intervening section, interact with one another and allochthonous bodies of the
63 older salt layer influence both the distribution and halokinetic structures formed in the younger
64 salt layer (Snidero et al., 2020; Hassanpour et al., 2021). Similarly, several basins across NW
65 Europe contain multiple, relatively thin (typically less than a few 100s of metres)
66 autochthonous layers of salt that form a variety of halokinetic structures. These include
67 Permian and Triassic salt layers in the Sole Bit Basin and the Danish Central Graben in the
68 North Sea (Stewart et al., 1996; McKie, 2017; Hansen et al., 2021) as well as multiple layers
69 of Triassic salt encountered in the Irish Sea basins (Quirk et al., 1999). The Slyne Basin
70 offshore NW Ireland is an ideal natural laboratory to observe the evolution of structures in a
71 basin with multiple thin salt layers (Fig. 1). Two main salt bodies have been proven in this
72 basin, the Upper Permian Zechstein Group and the Upper Triassic Uilleann Halite Member
73 (Fig. 2). Both of these salt layers have been active during the multiphase evolution of the basin
74 from the break-up of Pangea during the Permian through to the opening of the North Atlantic
75 during the Eocene (Dancer et al., 1999; Štolfová & Shannon, 2009; Stoker et al., 2017; Merlin
76 Energy Resources Consortium, 2020; O'Sullivan et al., 2021). Permian salt anticlines and
77 rollers have been recorded throughout the Slyne Basin, while observations of Triassic salt
78 walls and salt rollers are largely confined to the Northern Slyne Sub-basin (O'Sullivan et al.,

79 2021). The best studied structure in the area where both salt layers are present is the anticline
80 hosting the Corrib gas field in the Northern Slyne Sub-basin (Fig. 1).

81 The Corrib gas field contains circa 1 Tcf of gas and is one of Ireland's main indigenous sources
82 of energy (Dancer et al., 2005). Schematic models of the evolution of the structure have been
83 presented previously which presented the concept of 'double-decker' halokinesis (sensu
84 Corcoran & Mecklenburgh, 2005) and a reversal in polarity of the main fault in the supra-salt
85 overburden during different stages of syn-rift evolution (Fig. 2), beginning with a fault dipping
86 towards the NW during the Early to Middle Jurassic, followed by a fault dipping to the SE
87 during the Late Jurassic (Dancer et al., 2005). Subsequent acquisition of high-quality seismic
88 data and the drilling of additional wells provides the impetus for a reassessment of the
89 structural evolution of the Corrib gas field and the interaction between the stratigraphically
90 discrete layers of salt that formed the structural closure. Note also that the majority of the
91 section previously dated as Middle Jurassic (late Bajocian and Bathonian) in these previous
92 studies has been reclassified as Late Jurassic in age by a recent biostratigraphic study of the
93 Irish Atlantic margin (Merlin Energy Resources Consortium, 2020).

94 The results of this reassessment of the Corrib and adjacent structures has implications for the
95 evolution of structural traps in other rift basins which contain multiple relatively thin layers of
96 salt throughout their stratigraphy, such as those on the Irish Atlantic margin and across NW
97 Europe.

98 Geological Setting – The Slyne Basin

99 The Slyne Basin is a narrow, elongate rift basin located on the Irish Atlantic margin offshore
100 north-western Ireland (Fig. 1). The basin is 200 km long and varies between 20-60 km in width,
101 trending broadly NNE-SSW. The Irish Mainland Shelf bounds the Slyne Basin to the east,
102 while the Rockall Basin and Porcupine High form the western boundary. The Slyne Basin is
103 connected to the contiguous Erris Basin to the north, which is downthrown relative to Slyne
104 Basin across a large fault, while a narrow basement high separates the Slyne Basin from the
105 Porcupine Basin to the southwest (Chapman et al., 1999; O'Sullivan et al., 2021). The Slyne
106 Basin is divided into three sub-basins which are asymmetric half-grabens or grabens
107 (Trueblood & Morton, 1991). The asymmetry of these sub-basins varies along-strike, with
108 polarity changing across areas of structural complexity linked to underlying Caledonian
109 structural lineaments (Trueblood & Morton, 1991; Chapman et al., 1999; Dancer et al., 1999).
110 This study focuses on the Northern Slyne Sub-basin (Fig. 1).

111 Structural Evolution

112 The Slyne Basin is a series of interconnected half-grabens bounded by large faults which are
113 the product of a multiphase structural evolution stretching from the Late Permian to the mid
114 Cenozoic (Shannon, 1991; Dancer et al., 1999; Doré et al., 1999). Rifting began in the Late
115 Permian associated with the breakup of Pangea, followed by a period of tectonic quiescence
116 during the Triassic. A second phase of relatively low-strain extension began during the Early
117 Jurassic alongside a regional marine transgression, with extension continuing into the Middle
118 Jurassic followed by regional uplift and erosion during the late Middle Jurassic (Merlin Energy
119 Resources Consortium, 2020; O’Sullivan et al., 2021). The main phase of rifting began during
120 the Late Jurassic, with the faults bounding the Slyne Basin accumulating several kilometres
121 of throw, forming the NNE-SSW rift axis observed at present (Fig. 1A, Dancer et al., 1999;
122 Naylor & Shannon, 2005). In the Northern Slyne Sub-basin this resulting in a broad eastward
123 dip towards the basin-bounding faults along the eastern margin of this sub-basin (Fig. 1).
124 Rifting ceased at the end of the Jurassic and the region experienced kilometre-scale uplift and
125 erosion during the Early Cretaceous, creating a distinct regional unconformity (Dancer et al.,
126 1999; Corcoran & Mecklenburgh, 2005). The basin experienced minor extensional forces
127 during the Cretaceous, related to rifting in the neighbouring Rockall Basin, before a second
128 period of uplift created a second regional unconformity during the early Cenozoic (Chapman
129 et al., 1999; Dancer et al., 1999; Corcoran & Mecklenburgh, 2005). The entire Irish Atlantic
130 margin experienced significant magmatism related to the development of the North Atlantic
131 Igneous Province during the Paleocene and Eocene (Corcoran & Mecklenburgh, 2005; Meyer
132 et al., 2007; Magee et al., 2014), which manifested in the Slyne Basin as several sills that
133 intrude throughout the basin and extensive basaltic lava flows in the Northern and Southern
134 Slyne sub-basins (Fig. 1 & 3).

135 Stratigraphic Framework

136 The pre-Permian sedimentary fill of the Slyne Basin consists of a Pennsylvanian sequence of
137 sandstones and mudstones with interbedded coal horizons and a Mississippian sequence of
138 mudstones, sandstones and limestones (Fig. 3) underlain by Silurian metasediments (Tate &
139 Dobson, 1989; Merlin Energy Resources Consortium, 2020). The Permian section consists of
140 a sequence of mobile salt composed predominately of halite, which changes towards the basin
141 margins to a section dominated by clastic and carbonate lithologies (O’Sullivan et al., 2021).
142 This Permian section is a lateral equivalent to the Zechstein Group of NW Europe. The
143 overlying Lower Triassic Corrib Sandstone Formation consists of a near isopachous sequence
144 (c. 330 m) of fluvial sandstones interbedded with thin layers of red mudstones (Dancer et al.,

145 2005). These sandstones are overlain by an Upper Triassic section composed of red
146 mudstones with thin interbeds of sandstone and siltstones belonging to the Currach Formation
147 (Dancer et al., 1999). In the Northern Slyne Sub-basin a second layer of mobile halite is
148 present towards the base of the Upper Triassic section, termed the Uilleann Halite Member
149 (Merlin Energy Resources Consortium, 2020; O'Sullivan et al., 2021).

150 The Lower and Middle Jurassic sections in the Slyne Basin belong to the Lias and Kite groups
151 respectively and are dominated by marine mudstones interbedded with sandstones,
152 carbonates and thin layers of anhydrite (Trueblood & Morton, 1991; Dancer et al., 1999; Merlin
153 Energy Resources Consortium, 2020). The overlying Upper Jurassic section is composed of
154 several kilometres of fluvio-estuarine mudstones and sandstones belonging to the Minard
155 Formation, which grade upwards to marine mudstones of the Sybil and Dawros formations. A
156 major regional unconformity separates the Upper Jurassic section from the underlying Lower
157 and Middle Jurassic section, with this unconformity removing the Middle Jurassic and the
158 upper part of the Lower Jurassic section from the basin margins, with a more complete
159 stratigraphic section preserved towards the centre of the basin (Dancer et al., 1999).

160 A distinct angular unconformity separates the Jurassic section from the Cretaceous and
161 Cenozoic post-rift sections (Fig. 3). The Lower Cretaceous is composed of glauconitic
162 sandstones overlain by Upper Cretaceous limestones. In the Northern Slyne Sub-basin,
163 extensive Eocene-aged basaltic lava flows infill the karstified surface of the Upper Cretaceous
164 limestones, which are in turn overlain by an attenuated, poorly consolidated sequence of
165 Miocene to Recent mudstones and sandstones.

166 Dataset & Methodology

167 Dataset

168 This study focuses on two borehole-constrained 3D seismic reflection volumes from the
169 Northern Slyne Sub-basin. The first is the EN3D97-REPRO, which is a subset of the larger
170 E97IE11 3D survey acquired in 1997 which covers 660 km² of the Northern Slyne Sub-basin
171 (Fig. 1). This volume was reprocessed in 2012 and provides a marked improvement in data
172 quality over a 480 km² area directly overlying the Corrib gas field (Fig. 1, 4). The second
173 seismic volume is the 13SH3D volume, an ocean-bottom cable survey acquired between 2012
174 and 2013, covering 247 km² directly above the Corrib gas field (Fig. 1) which provides the
175 clearest image of the Lower Triassic reservoir section (Shannon, 2018). Additional 3D seismic
176 volumes and a single 2D seismic line to the east of Corrib (Fig. 1) were used to provide
177 regional context across the Northern Slyne sub-basin.

178 The Permian and Triassic section is encountered between 2200 to 5000 mMDBRT (c. 1500-
179 3500 ms TWTT) across most of the study area. Low frequencies of 10-15 Hz at this depth
180 along with high velocities of 4000-5000 ms⁻¹ gives a seismic resolution of 70-125 m (one-
181 quarter wavelength sensu Brown, 2011). Seismic data quality in the Northern Slyne Sub-basin
182 suffers due to the near-seabed geology, consisting of Eocene-aged Druid Formation basaltic
183 lava underlain by Cretaceous-aged limestone of the Chalk Group. These features create
184 strong multiple energy and degrade the seismic image throughout the study area (Dancer &
185 Pillar, 2001). Seismic sections are presented in European polarity (Brown, 2001), where a
186 positive downwards increase in acoustic impedance corresponds to a positive (red) reflection
187 event and a decrease corresponds to a negative (blue) reflection event. All sections are
188 vertically exaggerated by a factor of three (e.g. Fig. 4) and ball-ends are used to highlight
189 where a fault terminates within a certain stratigraphic package, while faults without ball-ends
190 are truncated by a younger unconformity.

191 The seismic database is integrated with data from all exploration, appraisal and production
192 wells in the Northern Slyne Sub-basin (Fig. 1A). To date, five exploration wells have been
193 drilled in the Northern Slyne Sub-basin (18/20-1, 18/20-7, 18/25-2, 19/8-1 and 19/11-1A) along
194 with seven appraisal and production wells from the Corrib gas field (18/20-2z, -3, -4, -5, -6z,
195 and 18/25-1 & -3). Data from these wells includes wireline logs, cuttings descriptions, time-
196 depth relationships, and core data from the Lower Triassic reservoir section. Additionally, a
197 single shallow borehole from the north of the study area (19/13-sb01) includes core data from
198 the Cenozoic section, providing greater insight into the near-seabed geology in the Northern
199 Slyne Sub-basin. Formation tops were constrained using the most recent biostratigraphic data
200 from the updated stratigraphic framework for offshore Ireland (Merlin Energy Resources
201 Consortium, 2020) and these were tied to the seismic dataset using time-depth relationships
202 in the form of checkshots.

203 Methodology

204 Five key seismic horizons were mapped across the study area (top Lower Triassic, top Upper
205 Triassic, base Upper Jurassic, base Cretaceous and base Cenozoic, Fig. 3) to create structure
206 and thickness maps (in ms TWTT). The top Lower Triassic represents the top of the main
207 reservoir unit in the study area. Because the reservoir interval is isopachous (c. 330 m thick),
208 its base is also a proxy for the top Permian. The top Upper Triassic represents the top of the
209 principal cap rock in the study area. The base Upper Jurassic horizon is a regional
210 unconformity and marks the boundary between sediments deposited in the first (Early-Middle
211 Jurassic) and second (Late Jurassic) syn-rift phases in the Slyne Basin. The base Cretaceous
212 is a regional angular unconformity marking the cessation of rifting in the Slyne Basin and the

213 first stage of post-rift deposition. The base Cenozoic is another regional unconformity and
214 represents the onset of thermal subsidence in the neighbouring Rockall Basin to the NW.
215 Time-thickness maps were generated between mapped horizons to analyse thickness
216 variations in syn- and post-rift sections and to provide qualitative constraints on the evolution
217 of faults and halokinetic structures.

218 To analyse brittle deformation in the Jurassic supra-salt section and its relationship to the
219 evolution of halokinetic structures throw-distance plots were created for the base Upper
220 Jurassic Unconformity, the Base Cretaceous Unconformity, and the top of the Druid Formation
221 (Early Eocene) on the main listric fault located above the Corrib anticline and other key faults.
222 The throw-distance plots were then overlain above strike-sections of concordant Triassic and
223 Permian salt structures to assess spatial correlation and kinematic coherence between the
224 discrete halokinetic structures and their overburden (Walsh & Watterson, 1991; Childs et al.,
225 1993). Measurements were taken every 10 crosslines (approximately intervals of 125m)
226 oriented perpendicular to the strike of the principal listric fault.

227 To carry out 2D structural restoration, a velocity model was created to convert seismic sections
228 from the time to depth domain. The layer model consisted of intervals defined by the seabed,
229 base Druid Formation (Base-Cenozoic Unconformity), base Cromer Knoll Group (Base-
230 Cretaceous Unconformity), base Minard Formation (Base Upper Jurassic Unconformity), top
231 Currach Formation (Upper Triassic), top Corrib Sandstone Formation (Lower Triassic) and top
232 Zechstein Group (Upper Permian). An initial interval velocity and k-factor (the change in
233 interval velocity with depth) were calculated for each interval using data from wells within the
234 EN3D97-REPRO seismic volume (Table 1).

235 Structural restoration was carried out on a NW-SE oriented representative seismic cross-
236 section through the Corrib gas field taken from the EN3D97-REPRO seismic volume.
237 Restoration was carried out using a combination of 2D decompaction and move-on-fault
238 algorithms for the Cenozoic, Cretaceous and Upper Jurassic sections, following established
239 methodologies for restoration in salt-influenced basins (Rowan, 1993; Roberts et al., 1998;
240 Rowan & Ratliff 2012; Macaulay, 2017). Estimations for missing Cretaceous and Upper
241 Jurassic sections (100 and 1400 metres respectively) were taken from Corcoran &
242 Mecklenburgh (2005). A combination of 2D decompaction, move-on-fault and unfolding by
243 flexural slip (i.e. constant bed length) algorithms was used to reconstruct the Early and Middle
244 Jurassic evolution of the Corrib structure during the early phases of halokinesis. Decompaction
245 is performed using the Sclater & Christie (1980) function with most of the Mesozoic section
246 being siliciclastic-dominated apart from the Late Cretaceous Chalk Group, which is carbonate-
247 dominated. Flexural isostasy was used to compensate for sedimentary loading, using a crustal

248 density of 2.75 g/m³ and a crustal thickness of 30 km (O'Reilly et al., 1995; Kimbell et al.,
249 2010). As no accurate base-salt horizon can be interpreted in the Northern Slyne sub-basin
250 on the data available to this study, a schematic representation is included on restored sections
251 indicating a possible sub-salt geometry, based on the interpretation of basement geometries
252 in other parts of the Slyne Basin. The impact of igneous intrusions on the sedimentary column
253 is another uncertainty (*sensu* Mark et al., 2019). While large intrusions are present throughout
254 the stratigraphy (Fig. 4) they make up a very small proportion of the stratigraphy encountered
255 by drilling in the study area (Merlin Energy Resources Consortium, 2020).

256 Results

257 Structural Configuration

258 The structure containing the Corrib gas field consists of three discrete elements which share
259 a linked evolution (Fig. 4, 5); the Lower Triassic section is folded by a Permian salt anticline,
260 creating a NE-SW trending anticline which is 12 km long and 5 km wide (Fig. 6). The anticline
261 is flanked by synclines to the NW and SE, with the synclinal trough to the SE being around
262 300 ms TWTT deeper. A small satellite closure is present 8 km north of the Corrib fold, forming
263 the 'Corrib North' faulted anticline drilled by the 18/20-7 well (Fig. 1). Due south of the Corrib
264 anticline is a fault-bounded basement high which was drilled by the 18/25-2 'Shannon' well
265 (Fig. 1). This high is bounded by a fault trending WNW-ESE which wraps around the high to
266 trend NE-SW (Fig. 1).

267 The overlying Upper Triassic salt forms a narrow, 8 km long salt wall trending NE-SW (Fig.
268 6D). This salt wall trends parallel to the fold axis of the underlying salt-cored fold, but is offset
269 from the apex of the fold by 1 km to the NW. The 18/20-2z and 18/20-6z wells penetrate the
270 salt wall at its thickest point (c. 600 ms TWTT), encountering 783 and 704 m of halite with
271 interbedded layers of red mudstone respectively (Merlin Energy Resources Consortium,
272 2020). This salt decreases in thickness away from the crest of the Corrib anticline, with the
273 Uilleann Halite Member making up only 13 m of the total 107 m of the Upper Triassic section
274 in the 18/20-7 well (Shell, 2011).

275 The Upper Triassic salt wall forms a roller in the footwall of a large SE-dipping listric fault
276 (termed the Corrib fault in this study) which soles out in the Upper Triassic salt and trends
277 parallel to the fold-axis of the Permian salt anticline in a NE-SW orientation (Fig. 4-6). A faulted
278 rollover in the hanging-wall of the Corrib fault is interpreted to have formed by salt-cored
279 folding of the Jurassic overburden by the Permian salt anticline, displaced by movement on
280 the Corrib fault. This rollover is deformed by a series of smaller antithetic and synthetic faults

281 which also sole out in the Upper Triassic salt (Fig. 5). The Corrib fault has a sigmoidal trace
282 in map view (Fig. 6C), where the north-eastern and south-western ends of the fault are
283 oriented ENE-WSW and oblique to the NE-SW orientation of the central portion of the fault
284 (Fig. 5). Three fault splays in the hanging wall of the Corrib fault are interpreted to represent
285 breached relay ramps (Fig. 5, 6C).

286 Unlike the Jurassic section, the post-rift sediments are largely undeformed, with a distinct
287 truncation of the folded Upper Jurassic sediments at the relatively flat-lying Base-Cretaceous
288 Unconformity (Fig. 4, 5). Both the Cretaceous and Cenozoic sections dip gently towards the
289 NW, likely a result of post-rift thermal subsidence in the neighbouring Rockall Basin during the
290 Cenozoic (Fig. 1) and are offset by normal movement on the Corrib fault (Fig. 4, 5). In addition
291 to the reactivation of the Corrib fault, a series of ENE-WSE oriented faults is observed
292 deforming the Cretaceous and Jurassic section 5 km to the SE of the Corrib structure (Fig.
293 6B), likely related to rifting in the Rockall Basin during the Cretaceous. Faults of a similar age,
294 magnitude and orientation have recently been identified in the Porcupine Basin to the SW of
295 the study area (Saqab et al., 2020). The Cretaceous faults in the Corrib area appear to have
296 been exploited by Cenozoic sills that intrude into the Upper Jurassic and Cretaceous
297 sediments to the SE of the Corrib structure, causing doming and folding in the overlying
298 Cretaceous sediments (Fig. 4, 6B, 7). These sills do not deform the base of the Druid
299 Formation lavas (dated 40-54.3 Ma, Dancer et al., 2005), with the crests of the sill-induced
300 folds eroded by the unconformity at the base of this section, indicating the sills pre-date the
301 extrusion of these early-mid Eocene volcanics. In addition to these sills which intrude into the
302 Upper Jurassic section directly beneath the Base-Cretaceous Unconformity, there are several
303 other intrusions observed in the Lower and Middle Jurassic section which may be coeval.
304 These deeper sills are more strata concordant when compared to the saucer shape
305 morphology of their shallower counterparts (Fig. 4).

306 Isochron analysis

307 The mapping of significant seismic horizons allows the vertical thickness of different
308 sedimentary packages to be calculated and displayed as isochron maps (in ms TWTT).
309 Isochrons were generated for the Upper Triassic (Currach Formation and Uilleann Halite
310 Member), Lower-Middle Jurassic (Penarth, Lias, and Kite groups), Upper Jurassic (Beara and
311 Muckcross groups), and Cretaceous (Cromer Knoll and Chalk groups) sections within the
312 EN973D-REPRO seismic volume (Fig. 8).

313 The elongate salt wall above the Corrib anticline is clearly visible on the Upper Triassic
314 isochron map, trending NE-SW parallel to the fold axis of the Lower Triassic salt-cored fold

315 (Fig. 8D). The Currach Formation thickens significantly into the hanging-wall of a N-S oriented
316 fault due east of the Corrib anticline, reaching thicknesses greater than 600 ms TWTT (Fig.
317 8D). As the throw on this fault is greater than the thickness of the Lower Triassic Corrib
318 Sandstone Formation, there may be mixing of Upper Triassic and Permian salt and mudstone
319 in the fault plane (Fig. 6, 8D). The Upper Triassic section also thickens in the syncline to the
320 NW of the Corrib anticline (Fig. 4, 8D). This suggests that halokinesis of the Permian salt may
321 have begun during the Late Triassic, possibly driven by active faults in the sub-salt basement.

322 The Lower and Middle Jurassic sections thicken into the synclines flanking the Corrib anticline
323 while they thin onto the crest of the fold (Fig. 8C). The sequence in the syncline to the NW is
324 c. 250 ms TWTT thicker than in the SE syncline, suggesting asymmetry in the salt-cored fold
325 during the Early and Middle Jurassic. The dislocation of the axis of the thickened Lower and
326 Middle Jurassic section relative to the Triassic depocenter mentioned above suggests that
327 halokinesis of the Triassic salt may have begun during this time (Fig. 4). The NW-SE oriented
328 fault south of Corrib was active during the Early and Middle Jurassic, and a significantly thinner
329 section of Lower and Middle Jurassic sediments are observed on the footwall of this fault block
330 (Fig. 8C).

331 The polarity of the depocenters changed during the Late Jurassic, with a significantly thicker
332 Upper Jurassic section present in the syncline to the SE (Fig. 8B). During this time there was
333 significant regional extension and movement on the basin-bounding faults to the SE of the
334 Corrib structure (Fig. 1D). Comparison with seismic sections shows a broad eastward fanning
335 of reflectors (Fig. 4) towards the basin-bounding fault system east of Corrib (Fig. 1) while there
336 is no clear indication of growth sequences in the hanging-wall of the Corrib fault (Fig. 4). The
337 inconsistency between the thickness changes recorded in the Upper Jurassic isochron (Fig.
338 8B) and reflector geometries on seismic sections can be explained by early Late Jurassic,
339 Beara Group deposition being primarily controlled by movement on the basin-bounding fault
340 system to the east of Corrib (Fig. 1), while growth of the Permian salt anticline occurred at a
341 later stage of Late Jurassic rifting, with evidence of this growth on the seismic data lost due to
342 post-rift erosion.

343 There is evidence of fault activity during both the Cretaceous and Cenozoic, with the
344 Cretaceous Cromer Knoll and Chalk groups thickening into the hanging wall of the Corrib fault,
345 as well as the ENE-WSE faults which formed during this time (Fig. 4, 5, 8A). The impact of the
346 Cenozoic sills is also observed on the Cretaceous isopach, with erosion above the SE syncline
347 where several sills intrude into the Upper Jurassic section directly beneath the Base
348 Cretaceous Unconformity (Fig. 7, 8A).

349 Fault analysis

350 The Corrib fault is a SE dipping listric fault which soles out in the Upper Triassic Uilleann Halite
351 Member and has a total length of 24 kilometres (Fig. 6, 9). The greatest throws on the fault
352 are almost 450 ms TWTT and occur at the base of the Upper Jurassic section (Fig 9A) The
353 cumulative throw of the fault and two large hanging wall splays is greater than 350 ms TWTT
354 for a 10-kilometre-long section at the centre of the fault directly overlying both the Upper
355 Triassic and Permian salt structures (Fig. 9A, B). The throw of the primary Corrib fault
356 decreases sharply to the SW from over 300 ms TWTT to under 50 ms TWTT over a kilometre,
357 with much of this strain being transferred to a breached relay zone (R1) and nearby faults (S1
358 and S2; Fig. 9A, E). There is a more gradual decrease in throw to the NE, where throw
359 decreases from 350 ms TWTT to 50 ms TWTT over four kilometres (Fig. 9A). The throw
360 distribution on the fault broadly correlates with the along-strike elevation at the Top Triassic
361 horizon (compare the cumulative throw curve in Fig. 8A with the Top Currach Formation
362 elevation in Fig. 9B) demonstrating a kinematic connection between fault offset and the
363 movement of the salt layers that has generated this topography.

364 Within the Jurassic section only the Base Upper Jurassic Unconformity can be used to
365 construct a throw profile, primarily because it is difficult to define Lower and Middle Jurassic
366 hanging wall cut-offs due to the listric fault geometry and the lack of continuous reflectors in
367 the Upper Jurassic section. Cross-sections through the fault and local well developed Lower
368 to Middle Jurassic reflectors (e.g. Fig. 4, 9E-G) do not indicate any appreciable growth of the
369 Corrib fault in this interval and the Lower and Middle Jurassic thickness variations adjacent to
370 the fault are related to salt movement or later structural thinning. The throw profile constructed
371 at the Base Upper Jurassic Unconformity is therefore thought to record most of the Jurassic
372 throw on this fault. Throw profiles with throw maxima of 50 ms TWTT and 150 ms TWTT (Fig.
373 9A) for the Druid Formation and Base Cretaceous Unconformity, respectively, record post-rift
374 resolvable reactivation along up to 20 km of the fault; sub resolution post-rift movement may
375 have occurred along its entire length. Comparison between the throw profiles for the different
376 offset horizons (Fig. 9A) demonstrates that most of the fault throw accumulated before the
377 deposition of the preserved Cretaceous section and simple backstripping of the post-rift fault
378 throw (Chapman & Meneilly, 1991; Petersen et al., 1992; Childs et al., 1993) indicates that the
379 cumulative throw on the Corrib fault towards the end of the Late Jurassic i.e. before post-rift
380 tectonic activity, was a maximum of 300-350 ms TWTT (Fig. 9C).

381 The jagged trace of the Corrib fault and three significant splays in the hanging wall of the fault
382 (Fig. 9D) indicate that the fault developed through linkage of a series of left-stepping faults
383 where the splays are the locations of earlier relay ramps that have been breached.

384 Approximate timing of the breaching of these relay zones can be estimated from the seismic
385 data and the fault throw profiles. The seismic data indicate that the hanging wall splays
386 terminate upwards within the Upper Jurassic section (Fig 9E-G) suggesting they became
387 inactive during this interval. The throw on the splays at the branchpoint with the throughgoing
388 fault (the Corrib fault) can also give an indication of the throw at which the relay ramps were
389 breached, and fault segments became connected. For both relay zones R2 and R3 the throw
390 on the splay where it intersects the main Corrib fault is 150 ms TWTT, while the throw on relay
391 zone R1 is 100 ms TWTT (Fig. 9A). This indicates that the R2 and R3 relay zones were
392 breached when the throw on the Corrib fault was 150 ms TWTT and more than half of its throw
393 at the end of the Jurassic. The pattern of left-stepping faults continues along-strike both north
394 and south of the Corrib fault, but at these locations the fault throw is insufficient to cause
395 breaching of the 1 to 3 km wide relay zones (e.g. S1 and S2, Fig. 9D).

396 The initiation of the Corrib fault as a series of left-stepping faults requires explanation. If the
397 fault formed in response to the rise of the Permian or Triassic salt structures alone then the
398 faults would be expected for form broadly parallel to their axes (i.e. oriented NE-SW).
399 However, the obliquity of the initial fault segments, which are oriented ENE-WSW, suggests
400 that extensional stresses unrelated to these structures played a significantly role in fault
401 initiation. These extensional stresses could be of direct tectonic origin. At the time of fault
402 initiation (during the Early to Middle Jurassic), the Jurassic section would have been
403 decoupled from the basement by both the Upper Triassic and Permian salt layers so that the
404 orientation of these faults may be a direct indicator for the Early Jurassic extension direction.
405 Alternatively, they could be of gravitational origin resulting from the SE tilting towards the
406 active basin-bounding fault. It is not possible to determine from the data whether the en
407 echelon fault array initiated during the relatively minor Early to Middle Jurassic or the main
408 Late Jurassic phase of rifting.

409 Although tectonically induced stresses, direct or indirect, are likely to have played a significant
410 role in the initiation of the Corrib fault, the main driver for the accumulation of throw is salt
411 movement as is apparent from the strong correlation between horizon elevation and fault throw
412 (Fig. 9A, B). The Upper Triassic and Permian salt layers provide two potential mechanisms
413 for driving fault movement. The first mechanism is gravity sliding on the flank of the rising
414 Permian salt anticline, where the Upper Triassic salt acts as a décollement accommodating
415 the downthrow of the hanging wall of the fault. The second mechanism is the relative uplift of
416 the footwall by growth of the Upper Triassic salt wall, which is supported by the seismic cross-
417 sections (Fig. 1, 4) and the Late Triassic isopach map (Fig. 8D). By comparing the topography
418 along the length of the fault with the fault throw distribution we can place some constraints on
419 the relative magnitudes of these two drivers.

420 The topography along a profile at the Top Currach Formation has two components: the
421 topography of the Permian salt anticline and the irregular thickness of the Upper Triassic salt
422 wall. The intervening isopachous Lower Triassic makes no contribution to topographic
423 variation. Were all throw on the fault due to inflation in its footwall, there should be a one-to-
424 one correspondence between the topographic contribution from the Upper Triassic salt and
425 the throw. However, the topographic contribution of the Upper Triassic salt is lower than the
426 total throw on the Corrib fault along its entire length by between 100 and 200 ms TWTT (Fig.
427 9C). The excess throw is considered to be driven predominantly by growth of the Permian salt
428 anticline in response to tectonic forces related to the high-strain regional extension in the Late
429 Jurassic, although there is also likely to be some contribution from outer-arc extension due to
430 the Permian salt anticline. The Triassic salt thickness and associated contribution to throw
431 from the salt wall is greatest at the centre of the Corrib fault, where it accounts for 300 of the
432 400 ms TWTT total throw (Fig. 9A-C) while north and south only 100 ms of the throw can be
433 attributed to the salt wall. This pattern can be rationalised in terms of the respective
434 wavelengths of the Permian and Upper Triassic salt structures; the Permian salt anticline
435 extends beyond the Triassic salt wall both to the north and south, indicating the rise of Permian
436 salt is the driver for fault movement on the northern and southern ends of the fault, with a
437 progressive decrease in amplitude of the Permian salt anticline reflected in the reduced fault
438 throw.

439 A notable feature of previous interpretations of the Corrib structure was faults antithetic to the
440 Corrib fault. These faults have been interpreted as an Early Jurassic listric fault which dipped
441 towards the NW before the polarity of the Corrib fault changed to that observed at present
442 (Fig. 2, Dancer et al., 2005; Corcoran & Mecklenburgh, 2005). Modern seismic data reveals
443 that most of these faults are not through going and are instead comprised of two discrete fault
444 families; a lower set of faults which offset horizons within the Lower and Middle Jurassic
445 section and generally terminate upwards in the Upper Jurassic section (Fig. 4, 9D), and a
446 second set of faults offsetting Cretaceous and Jurassic horizons before being truncated by the
447 Base Cenozoic Unconformity (Fig. 4). The former group of faults were likely to have been
448 active during the early Late Jurassic, while the latter were active during the Cretaceous and
449 Cenozoic. Polarity reversal of the Corrib fault is also difficult to justify with the evidence
450 presented above.

451 Evolution of the Corrib structure

452 Structural restoration was performed on a representative seismic section across the Corrib
453 structure (Fig. 10) using the context provided by observations described above. As the pre-
454 salt basement is not clearly imaged within the study area, a schematic basement geometry

455 was included in each stage of the structural restoration to showcase the potential influence
456 basement geometry had on halokinesis and structural evolution, using context from other
457 areas of the Slyne Basin (e.g. Trueblood & Morton, 1991; Dancer et al., 1999; O'Sullivan et
458 al., 2021).

459 The Early Triassic Corrib Sandstone Formation is largely isopachous throughout the Slyne
460 Basin (Fig. 4, Merlin Energy Resources Consortium, 2020) indicating a period of tectonic
461 quiescence in the area. Thickening of the Currach Formation to the NW of Corrib (Fig. 4, 8D)
462 suggests that the movement of Permian salt began during the Late Triassic, likely driven by
463 active faulting in the sub-salt basement (Fig. 10A). Evidence for Late Triassic fault activity in
464 the Slyne Basin has not been reported previously but has been observed in other areas
465 including the Erris, Larne and Kish Bank basins (Chapman et al., 1999; Dunford et al., 2001;
466 Fyfe et al., 2020). The Triassic depocenter suggests this Late Triassic extension may have
467 extended to the Slyne Basin.

468 A relatively isopachous section of interbedded shallow marine mudstones, sandstones and
469 limestones were deposited in the Northern Slyne Sub-basin during the Hettangian to
470 Sinemurian (Fig. 11). A stratigraphic break occurred towards the end of the Pliensbachian,
471 forming a minor regional angular unconformity above the crest of the incipient Permian salt
472 anticline (Fig. 4, 10C, 11). This was followed by the deposition of a thicker section of Toarcian
473 and Middle Jurassic sediments in the synclines to the NW and the SE (Fig. 8C, 10D, 11).

474 A well correlation through the three wells which penetrate a complete Lower and Middle
475 Jurassic section within the EN3D97-REPRO seismic volume highlights both the thickening of
476 this section in the syncline to the NW as well as the erosion and reduced section present
477 across the crest of the salt-cored fold (Fig. 11). A circa 300 m section of the Pabay Shale
478 Formation has been eroded at the 18/25-1 well location, while a conformable contact is
479 observed between the Whitby Mudstone and Pabay Shale formations in both the 18/20-1 and
480 18/20-7 wells (Merlin Energy Resources Consortium, 2020). Additionally, a thinned section of
481 Whitby Mudstone Formation is present on the crest of the salt-cored fold that is roughly half
482 the thickness of the section recorded off-structure. The broadly isopachous Inagh, Meelagh
483 and Conn formations observed across the area indicates that there was little salt movement
484 during the Hettangian and Sinemurian (Fig. 11). The array of ENE-WSE oriented fault
485 segments that preceded the Corrib fault likely began forming during the late Early and Middle
486 Jurassic, driven by regional extensional stresses (Fig. 10D)

487 A stratigraphic break occurred during the Bathonian and Callovian along with local erosion, to
488 form the regional Base Upper Jurassic Unconformity observed throughout the Slyne Basin
489 (Merlin Energy Resources Consortium, 2020). High-strain regional extension during the Late

490 Jurassic resulted in the faults bounding the Northern Slyne Sub-basin along its eastern margin
491 accumulating several kilometres of throw (Fig. 1E) resulting in a relatively steep sub-salt basin
492 tilt into the hanging walls of these faults (Fig. 10E). The asymmetry of the salt-cored fold would
493 have changed as a result, with a thicker Upper Jurassic section being deposited in the syncline
494 to the SE adjacent to the active basin-bounding fault (Fig. 8). Sediment loading in the
495 immediate hanging-wall of the basin-bounding fault (i.e. the SE syncline) would have resulted
496 in the movement of Permian salt into the Corrib salt anticline and ultimately welding of the
497 Lower Triassic and Carboniferous basement (Fig. 10E). Sediment loading in the synclines
498 flanking the anticline likely triggered halokinesis in the Upper Triassic salt, from the synclines
499 towards the crest of the fold. The combination of high-strain extensional stresses and the
500 thickening of the Upper Triassic salt along the crest of the salt-cored fold led to the reactivation
501 of the Early-Middle Jurassic fault system, forming the Corrib fault through fault linkage and the
502 breaching of relay ramps (Fig. 10J), downthrowing the axis of the folded Jurassic section to
503 the SE (Fig. 10E). Outer-arc extension, due to the rising Permian salt anticline, is likely to have
504 contributed to the total throw of the Corrib fault.

505 The Slyne Basin experienced kilometre-scale uplift and erosion as rifting ceased at the end of
506 the Jurassic. Corcoran & Mecklenburgh (2005) estimate over a kilometre of the Upper Jurassic
507 section was removed above the Corrib anticline during the Early Cretaceous (Fig. 10F), and
508 that there may have been movement on the Corrib fault during this period of exhumation.
509 Following this regional uplift and erosion, a relatively thin section of Cretaceous sediments
510 was deposited across the Northern Slyne Sub-basin. The Corrib fault was reactivated during
511 the deposition of both the Early and Late Cretaceous sections with growth strata observed in
512 the hanging wall, while a series of shallow faults oriented NE-SW formed during the Late
513 Cretaceous above the crest of the Jurassic rollover in the hanging wall of the Corrib fault (Fig.
514 4, 9, 10G, H). This post-rift activity on the Corrib fault was likely caused by modification of the
515 Permian and Triassic salt structures driven by regional tectonic events such as rifting and
516 hyperextension in the neighbouring Erris and Rockall basins to the NW (Knott et al., 1993;
517 Chapman et al., 1999; Zeigler & Dèzes, 2006). The ENE-WSW faults located to the SE of
518 Corrib also formed during this time (Fig. 6, 8, 10G, H).

519 A second phase of regional uplift and erosion occurred during the early Cenozoic with an
520 estimated 50-150 metres of Late Cretaceous sediments removed above the Corrib structure
521 (Corcoran & Mecklenburgh, 2005). Several sills intruded into the Mesozoic section throughout
522 the Slyne Basin during the early Cenozoic; at depth these sills were concordant with the Lower
523 and Middle Jurassic stratigraphy (Fig. 4, 9E), while those intruding into the shallow Upper
524 Jurassic and Cretaceous section caused folding and faulting, with the crests of sill-induced
525 folds eroded during this phase of uplift (Fig. 7). Several of these sills have a stepped

526 morphology likely due to rising magma utilising Cretaceous-aged, ENE-WSW faults as
527 migration pathways. The lavas of the Druid Formation were extruded onto this early Cenozoic
528 unconformity across the Northern Slyne Sub-basin and appear to post-date the sill-related
529 folding and deformation (Fig. 7). The Corrib fault was reactivated for a second time during this
530 time, with a thicker section of Druid Formation and overlying Hebrides Margin and Eilean Siar
531 group sediments preserved in the hanging wall (Fig. 4, 5, 10I). Thermal subsidence in the
532 hyperextended Rockall Basin occurred during this time (Chapman et al., 1999; Doré et al.,
533 1999) and was likely the strongest driver of Cenozoic post-rift deformation, with differential
534 subsidence occurring along the NW margin of the Slyne basin, most evident on a regional
535 transect of the Northern Slyne Sub-basin (Fig. 1D).

536 Discussion

537 Revised structural evolution of the Corrib gas field

538 Previous models for the structural evolution of the Corrib structure proposed that the polarity
539 of the Triassic salt roller and resultant listric fault changed during the evolution of the structure
540 (Fig. 2, Corcoran & Mecklenburgh, 2005; Dancer et al., 2005). They have interpreted a fault
541 dipping to the NW prevailing during the Early and Middle Jurassic before a polarity reversal
542 resulted in the SE dipping fault during the Late Jurassic observed at present. This is based on
543 the interpretation of erosion and a missing section of the Lower and Middle Jurassic section
544 on the SE flank of the Corrib structure (Corcoran & Mecklenburgh, 2005; Dancer et al., 2005).
545 These authors interpreted the erosion as the product of a 'Base-Middle Jurassic Unconformity'
546 and is equivalent to the unconformity observed at the base of the Whitby Mudstone Formation
547 observed over the crest of the Corrib structure (Fig. 2, 4), dated as late Pliensbachian to early
548 Toarcian in the revised stratigraphic framework for offshore Ireland (Merlin Energy Resources
549 Consortium, 2020).

550 On modern seismic data this erosion is relatively subtle and is symmetrical, with erosion and
551 reflector truncation observed on both the NW and SE flank of the salt cored fold (Fig. 4). The
552 impact of this erosion is recorded in the 18/25-1 well on the crest of the Corrib anticline, where
553 circa 300 m of the Pabay Shale Formation is absent and is overlain by a reduced Whitby
554 Mudstone Formation relative to the stratigraphy encountered off structure (Fig. 11). Given the
555 relatively structural immaturity (*sensu* Jackson & Talbot, 1991; Hudec & Jackson, 2007) of the
556 salt structures observed in the Northern Slyne Sub-basin, the symmetrical erosion pattern is
557 more readily associated with the less complex growth of a salt anticline, where the crest of a
558 salt-cored fold can be eroded (Stewart & Coward, 1995; Hudec & Jackson, 2017). While
559 polarity reversal of large listric faults adjacent to rising salt diapirs is observed, it is more

560 commonly observed in structurally mature salt diapirs (e.g. Quirk & Pilcher, 2012).
561 Nevertheless, the asymmetry and variation in thickness between the Upper Jurassic and
562 Lower to Middle Jurassic sections observed by previous authors is confirmed in this study as
563 a product of halokinesis.

564 The kinematic interaction between discrete salt layers and Corrib 565 analogues in the Slyne Basin

566 The distinctive structure of the Corrib gas field formed through the combined effects of salt
567 migration in two distinct salt layers. The throw on the Corrib fault was driven by two different
568 but interdependent halokinetic processes, the listric nature of the hanging-wall and footwall
569 inflation. The relative importance of these mechanisms varies along the length of the Corrib
570 structure and may also have varied through time. There are a number of Corrib-like anticlinal
571 structures within the Northern Slyne Sub-basin (Fig. 12A, B, C). While these deform the same
572 stratigraphic template and have features in common with the Corrib structure, they also display
573 a varied response to the pillowing of Permian salt.

574 The Cong structure most closely resembles the Corrib gas field (Fig. 1A, 12A). It has a similar
575 structural geometry and scale, being a 15 km long and 5 km wide fold at Lower Triassic level
576 cored by a Permian salt anticline (Fig. 1A, 12A). In common with Corrib, a listric fault cuts
577 across the anticline, offsets the Jurassic overburden and soles out in the Upper Triassic salt.
578 Unlike Corrib the listric fault was not active after the Middle Jurassic and terminates at the
579 Base Upper Jurassic Unconformity despite the similarity in amplitude of these two structures.
580 A possible explanation for the lack of Late Jurassic faulting in the Cong structure is that, unlike
581 Corrib (Fig. 1B, 4), there was no tectonically induced tilting of the sub-salt basement during
582 the Late Jurassic.

583 A second structure of similar scale is Inishkea West which lies 20 km to the west of Corrib
584 (Fig. 1A, 12B). In this case, listric faults occur on both flanks of the Permian salt anticline,
585 dipping away from the crest rather than cutting across it and extend upwards to the Base
586 Cretaceous Unconformity. The fault on the western flank is much larger than those on the
587 eastern flank, and the offset is far larger than would be expected due to gravity sliding related
588 to the growth of the Permian salt anticline. This west dipping fault must have achieved its
589 displacement in response to the westward tilting of the basin following its initiation on the flank
590 of the Permian salt anticline.

591 Other variations in the style of deformation in the Slyne Basin can be seen by inspection of
592 Fig. 1D. A low amplitude salt anticline, Corrib North, shows subtle Lower-Middle Jurassic

593 thinning onto the anticlinal crest but no evidence for the formation of a listric fault (Fig. 12C).
594 In contrast to Corrib North, and 8 km to the NW, is a large (500 ms TWTT throw) listric fault
595 that soles out in the Upper Triassic salt, with thickened Upper Triassic salt in the footwall but
596 no obvious thickening in the underlying Permian. These two structures demonstrate that the
597 processes that drove the formation of the Corrib structure, and presumably also Cong and
598 Inishkea West, can also occur individually.

599 It is tempting to consider the Corrib North, Cong, Corrib and Inishkea West structures as
600 illustrating development stages of Permian salt anticline growth and the initiation of listric faults
601 during the Early-Mid Jurassic followed by Late Jurassic tectonic induced tilting leading to
602 increased throw on the listric faults. However, this is likely an oversimplification as the
603 evolution of structures is influenced by multiple interacting factors including variations in
604 primary salt thickness and welding of different salt layers.

605 Kinematic interaction between discrete layers of salt

606 Several basins across NW Europe, particularly those within the Southern Permian Basin, have
607 a similar stratigraphic configuration to the Slyne Basin and contain both Permian and Upper
608 Triassic salt layers. These include the Sole Pit and Lower Saxony basins and the Danish
609 Central Graben (Stewart et al., 1996; Kockel, 2003; Duffy et al., 2013). Relative to the Slyne
610 Basin, these areas have layers of Permian salt over a kilometre thick (Jackson & Stewart,
611 2017) while Triassic salt layers is restricted to layers thinner than 100 metres within a
612 mudstone-dominated section (McKie, 2017). Nevertheless, analogues to the Corrib gas field
613 are observed; the most striking of these is the Kraka salt pillow in the Danish Central Graben
614 (Fig. 12D). This structure consists of a Permian salt pillow of similar dimensions to Corrib (8
615 km wide and 10 km long with an amplitude of circa 1 kilometre) which folds the overlying
616 Mesozoic stratigraphy coupled with listric faulting soling out in layers of Triassic salt (Duffy et
617 al., 2013; Hansen et al., 2021). Small rollers of Triassic salt are also observed beneath the
618 footwalls of these listric faults (Fig. 12D). The Corrib and Kraka structures differ in the manner
619 of their later post-rift reactivation; the Corrib structure is subjected to extensional deformation
620 associated with nearby hyperextension and thermal subsidence in the Rockall Basin (Fig. 4),
621 while the Kraka structure is impacted by compressional tectonics (Fig. 12D) driven by the
622 Alpine Orogeny. Nevertheless, their pre-inversion geometries are near-identical (Hansen et
623 al., 2021 Figure 14 therein).

624 The variety of structures observed in the Northern Slyne Sub-basin and further afield
625 demonstrates that while the interaction of salt layers likely follows a similar geological evolution
626 early in their genesis, as strain values increase their evolution diverges. Where two layers of

627 salt are present in the stratigraphy of a rift basin, the older salt typically begins to flow first,
628 possibly before the deposition of the second layer. Salt flow and the formation of halokinetic
629 structures in the older salt creates topography that will influence and localise the formation of
630 secondary halokinetic structures in the younger salt layer. As these structures continue to
631 evolve factors such as local salt thickness, basin geometry and post-rift deformation result in
632 greater variation. Within the Northern Slyne Sub-basin the style of deformation is largely
633 controlled by these considerations but also the degree of tectonic tilting with increasing
634 tectonic strain that determines the extent to which the listric faults are amplified.

635 Conclusions

636 Using modern, borehole-constrained 3D seismic reflection data a detailed model of the Corrib
637 gas field offshore NW Ireland and its structural evolution has been developed. The Corrib gas
638 field consists of three principal components:

- 639 • A relatively simple NE-SW trending salt-cored fold at the Lower Triassic stratigraphic level
640 above a Permian salt anticline.
- 641 • An Upper Triassic salt wall trending parallel to the underlying salt-cored fold.
- 642 • A complex overburden of Jurassic syn-rift and Cretaceous and Cenozoic post-rift
643 sediments deformed by a listric fault (the Corrib fault) which dips towards the SE and
644 soles out in the Upper Triassic salt.

645 The multiphase structural evolution of the Corrib gas field is a result of rifting in the Slyne Basin
646 during the Late Triassic, Early to Middle Jurassic and Late Jurassic, followed by post-rift
647 deformation in the Cretaceous and Cenozoic:

- 648 1. The structure initiates with movement of the Permian salt during the Late Triassic and
649 the formation of a thickened Upper Triassic depocenter NW of the Permian salt
650 anticline, possibly driven by faulting in the sub-salt basement before tectonic
651 quiescence ensues during the earliest Jurassic.
- 652 2. Mild regional extension results in salt movement recommencing during the late Early
653 Jurassic with the growth of the Permian salt anticline and initiation of an Upper Triassic
654 salt anticline, both of which fold the overlying Jurassic sediments. This salt-cored fold
655 is asymmetric, with a thicker depocenter forming in the syncline to the NW. An oblique
656 array of en echelon faults forms in the Jurassic section due to regional extension.
- 657 3. The main phase of rifting occurs during the Late Jurassic with kilometre-scale
658 movement on the faults bounding the Northern Slyne Sub-basin. Basement tilting
659 towards the SE results in a reversal in the asymmetry of the salt-cored fold, with a
660 thicker depocenter developing in the syncline to the SE. A combination of regional

661 extensional forces and sediment loading inflates the Permian salt anticline. The pre-
662 existing fault system in the Jurassic section is reactivated as a major listric fault (the
663 Corrib fault) through the breaching of relay ramps and segment linkage, down throwing
664 the anticlinal crest of the Jurassic salt-cored fold towards the SE. As extension
665 continues, Upper Triassic salt forms an inflated, elongate salt roller in the footwall of
666 the Corrib fault, with sediment loading causing movement of Triassic salt from the
667 flanking synclines towards the crest of salt-cored fold. The final throw distribution on
668 the Corrib fault is a response to both inflation of Upper Triassic salt in the footwall and
669 regional extensional forces, with minor contributions in the form of outer-arc extension
670 and gravity gliding off the crest of the salt-cored fold.

671 4. Following the cessation of the rifting at the end of the Jurassic, the Northern Slyne
672 Sub-basin experiences kilometre-scale uplift and erosion. Rifting in the neighbouring
673 Rockall Basin results in reactivation of the Corrib fault and the modification of
674 halokinetic structures.

675 5. Post-rift thermal subsidence in the Rockall Basin results in differential subsidence
676 along the western margin of the Northern Slyne Sub-basin. The Corrib fault is
677 reactivated for a second time. At the same time, sills intrude throughout the Mesozoic
678 section in the area, followed by the extrusion of lavas across the Northern Slyne Sub-
679 basin during the Early Eocene.

680 The evolution of the Corrib structure demonstrates kinematic interaction between multiple salt
681 layers. Other anticlinal features in the Northern Slyne Sub-basin also demonstrate thin-
682 skinned deformation soling out in the Upper Triassic salt, above rising Permian salt structures
683 driven by a combination of regional tectonic forces and sedimentary loading. While
684 demonstrating the same two-salt deformation features, the variation between these structures
685 can largely be attributed to the magnitude of local Late Jurassic tilting and the regional
686 variation in salt thickness.

687 **References**

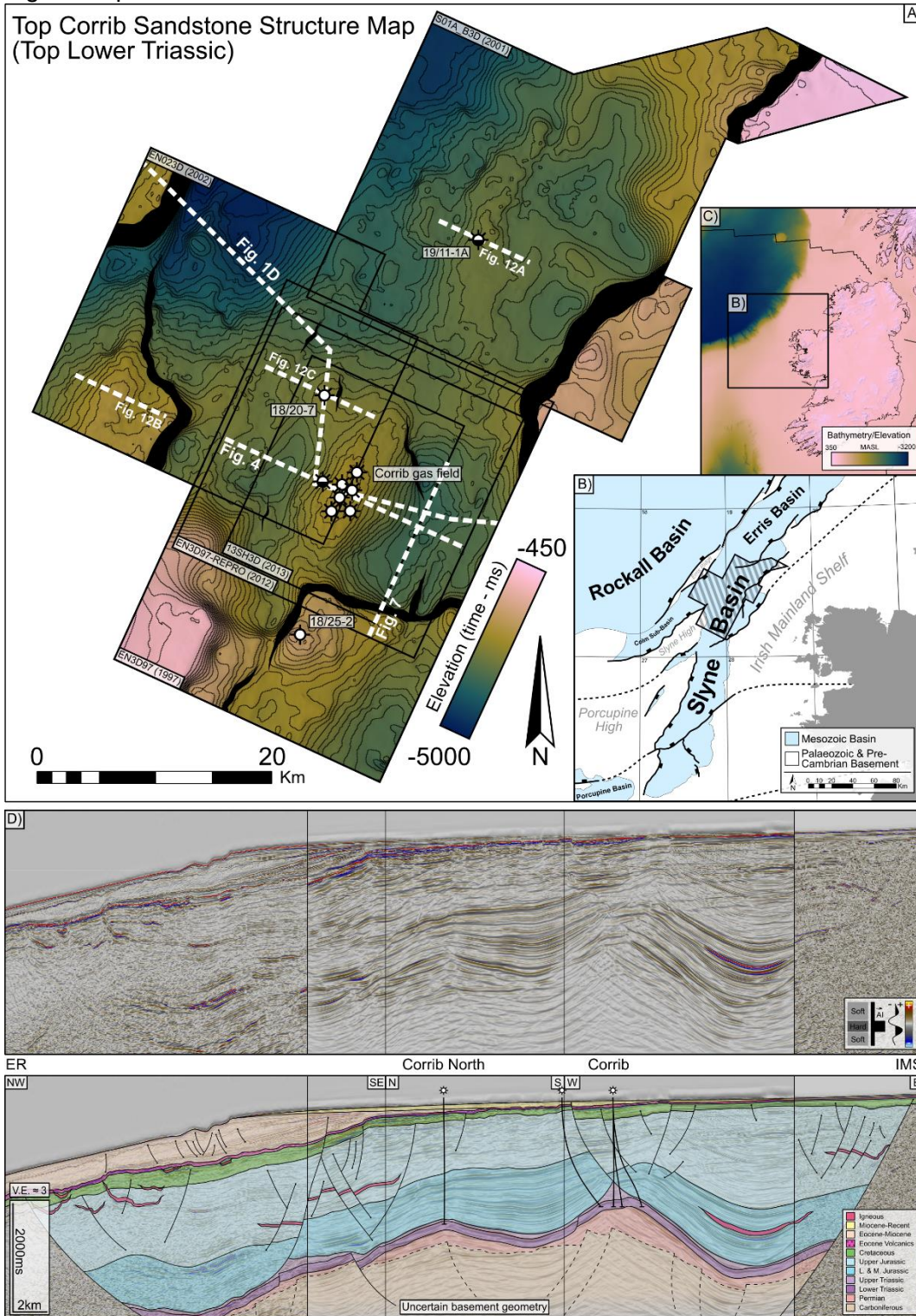
- 688 Chapman, T.J., Broks, T.M., Corcoran, D. V., Duncan, L.A. & Dancer, P.N. 1999. The
689 structural evolution of the Erris Trough, offshore northwest Ireland, and implications for
690 hydrocarbon generation. *Petroleum Geology of Northwest Europe: Proceedings of the*
691 *5th Conference*, 455–469.
- 692 Chapman, T.J. & Meneilly, A.W. 1991. The displacement patterns associated with a reverse-
693 reactivated, normal growth fault. *Geological Society, London, Special Publications*, **56**,
694 183–191, <https://doi.org/10.1144/GSL.SP.1991.056.01.12>.
- 695 Childs, C., Easton, S.J., Vendeville, B.C., Jackson, M.P.A., Lin, S.T., Walsh, J.J. &
696 Watterson, J. 1993. Kinematic analysis of faults in a physical model of growth faulting
697 above a viscous salt analogue. *Tectonophysics*, **228**, 313–329,
698 [https://doi.org/10.1016/0040-1951\(93\)90346-L](https://doi.org/10.1016/0040-1951(93)90346-L).
- 699 Corcoran, D. V & Mecklenburgh, R. 2005. Exhumation of the Corrib Gas Field, Slyne Basin,
700 offshore Ireland. *Petroleum Geoscience*, **11**, 239–256, <https://doi.org/10.1144/1354-079304-637>.
- 702 Dancer, P.N., Algar, S.T. & Wilson, I.R. 1999. Structural evolution of the Slyne Trough.
703 *Petroleum Geology of Northwest Europe: Proceedings of the 5th Conference on the*
704 *Petroleum Geology of Northwest Europe*, **1**, 445–454, <https://doi.org/10.1144/0050729>.
- 705 Dancer, P.N. & Pillar, N.W. 2001. Exploring in the Slyne Basin: a geophysical challenge. *The*
706 *Petroleum Exploration of Ireland's Offshore Basins*, **188**, 209–222,
707 <https://doi.org/10.1144/GSL.SP.2001.188.01.12>.
- 708 Dancer, P.N., Kenyon-Roberts, S.M., Downey, J.W., Baillie, J.M., Meadows, N.S. & Maguire,
709 K. 2005. The Corrib gas field, offshore west of Ireland. *Geological Society, London,*
710 *Petroleum Geology Conference series*, **6**, 1035–1046, <https://doi.org/10.1144/0061035>.
- 711 Davison, I. 2007. Geology and tectonics of the South Atlantic Brazilian salt basins.
712 *Geological Society Special Publication*, **272**, 345–359,
713 <https://doi.org/10.1144/GSL.SP.2007.272.01.18>.
- 714 Deptuck, M.E. & Kendell, K.L. 2017. A Review of Mesozoic-Cenozoic Salt Tectonics Along
715 the Scotian Margin, Eastern Canada. *In: Permo-Triassic Salt Provinces of Europe,*
716 *North Africa and the Atlantic Margins*. 287–312., <https://doi.org/10.1016/B978-0-12-809417-4.00014-8>.
717
- 718 Dooley, T.P., Hudec, M.R., Pichel, L.M. & Jackson, M.P.A. 2018. The impact of base-salt
719 relief on salt flow and suprasalt deformation patterns at the autochthonous,
720 paraautochthonous and allochthonous level: insights from physical models. *Geological*
721 *Society, London, Special Publications*, **476**, <https://doi.org/10.1144/SP476.13>.
- 722 Dooley, T.P., Jackson, M.P.A. & Hudec, M.R. 2013. Coeval extension and shortening above
723 and below salt canopies on an uplifted, continental margin: Application to the northern
724 Gulf of Mexico. *AAPG Bulletin*, **97**, 1737–1764, <https://doi.org/10.1306/03271312072>.

- 725 Doré, A.G., Lundin, E.R., Jensen, L.N., Birkeland, O., Eliassen, P.E. & Fichler, C. 1999.
726 Principal tectonic events in the evolution of the northwest European Atlantic margin.
727 *Petroleum Geology of Northwest Europe: Proceedings of the 5th Conference*, 41–61.
- 728 Doré, A.G., Corcoran, D. V. & Scotchman, I.C. 2002. Prediction of the hydrocarbon system
729 in exhumed basins, and application to the NW European margin. *Geological Society*
730 *Special Publication*, **196**, 401–429, <https://doi.org/10.1144/GSL.SP.2002.196.01.21>.
- 731 Duffy, O.B., Gawthorpe, R.L., Docherty, M. & Brocklehurst, S.H. 2013. Mobile evaporite
732 controls on the structural style and evolution of rift basins: Danish Central Graben,
733 North Sea. *Basin Research*, **25**, 310–330, <https://doi.org/10.1111/bre.12000>.
- 734 Dunford, G.M., Dancer, P.N. & Long, K.D. 2001. Hydrocarbon potential of the Kish Bank
735 Basin: Integration within a regional model for the Greater Irish Sea Basin. *Geological*
736 *Society Special Publication*, **188**, 135–154,
737 <https://doi.org/10.1144/GSL.SP.2001.188.01.07>.
- 738 Fyfe, L.-J.C., Schofield, N., Holford, S.P., Heafford, A. & Raine, R. 2020. Geology and
739 petroleum prospectivity of the Larne and Portpatrick basins, North Channel, offshore
740 SW Scotland and Northern Ireland. *Petroleum Geoscience*,
741 <https://doi.org/10.1144/petgeo2019-134>.
- 742 Hansen, T.H., Clausen, O.R. & Andresen, K.J. 2021. Thick- and thin-skinned basin inversion
743 in the Danish Central Graben, North Sea – the role of deep evaporites and basement
744 kinematics. *Solid Earth*, **12**, 1719–1747, <https://doi.org/10.5194/se-12-1719-2021>.
- 745 Hassanpour, J., Yassaghi, A., Muñoz, J.A. & Jahani, S. 2021. Salt tectonics in a double salt-
746 source layer setting (Eastern Persian Gulf, Iran): Insights from interpretation of seismic
747 profiles and sequential cross-section restoration. *Basin Research*, **33**, 159–185,
748 <https://doi.org/10.1111/bre.12459>.
- 749 Hudec, M.R. & Jackson, M.P.A. 2007. Terra infirma: Understanding salt tectonics. *Earth-*
750 *Science Reviews*, **82**, 1–28, <https://doi.org/10.1016/j.earscirev.2007.01.001>.
- 751 Jackson, C.A.-L. & Stewart, S.A. 2017. Composition, Tectonics, and Hydrocarbon
752 Significance of Zechstein Supergroup Salt on the United Kingdom and Norwegian
753 Continental Shelves. In: *Permo-Triassic Salt Provinces of Europe, North Africa and the*
754 *Atlantic Margins*. 175–201., <https://doi.org/10.1016/B978-0-12-809417-4.00009-4>.
- 755 Jackson, M.P.A. & Talbot, C.J. 1991. A glossary of salt tectonics. **91**. Bureau of Economic
756 Geology, University of Texas at Austin.
- 757 Jackson, M.P.A., Hudec, M.R. & Dooley, T.P. 2010. Some emerging concepts in salt
758 tectonics in the deepwater Gulf of Mexico: Intrusive plumes, canopy-margin thrusts,
759 minibasin triggers and allochthonous fragments. *Petroleum Geology Conference*
760 *Proceedings*, **7**, 899–912, <https://doi.org/10.1144/0070899>.
- 761 Jackson, M.P.A. and Hudec, M.R. 2017. Salt Pillows and Salt Anticlines. In: *Salt Tectonics*.
762 62–75., <https://doi.org/10.1017/9781139003988.007>.
- 763 Kimbell, G.S., Ritchie, J.D. & Henderson, A.F. 2010. Three-dimensional gravity and
764 magnetic modelling of the Irish sector of the NE Atlantic margin. *Tectonophysics*, **486**,
765 36–54, <https://doi.org/10.1016/j.tecto.2010.02.007>.

- 766 Knott, S.D., Burchell, M.T., Jolley, E.J. & Fraser, A.J. 1993. Mesozoic to Cenozoic plate
767 reconstructions of the North Atlantic and hydrocarbon plays of the Atlantic margins.
768 *Petroleum Geology of Northwest Europe: Proceedings of the 4th Conference*, 953–974,
769 <https://doi.org/10.1144/0040953>.
- 770 Kockel, F. 2003. Inversion structures in Central Europe - Expressions and reasons, an open
771 discussion. *Geologie en Mijnbouw/Netherlands Journal of Geosciences*, **82**, 367–382,
772 <https://doi.org/10.1017/s0016774600020187>.
- 773 Macaulay, E.A. 2017. A new approach to backstripping and sequential restoration in subsalt
774 sediments. *AAPG Bulletin*, **101**, 1385–1394, <https://doi.org/10.1306/11291616122>.
- 775 Magee, C., Jackson, C.A.L. & Schofield, N. 2014. Diachronous sub-volcanic intrusion along
776 deep-water margins: Insights from the Irish Rockall Basin. *Basin Research*, **26**, 85–105,
777 <https://doi.org/10.1111/bre.12044>.
- 778 Mark, N., Schofield, N., Gardiner, D., Holt, L., Grove, C., Watson, D., Alexander, A. & Poore,
779 H. 2019. Overthickening of sedimentary sequences by igneous intrusions. *Journal of*
780 *the Geological Society*, **176**, 46–60, <https://doi.org/10.1144/jgs2018-112>.
- 781 McKie, T. 2017. Paleogeographic Evolution of Latest Permian and Triassic Salt Basins in
782 Northwest Europe. In: *Permo-Triassic Salt Provinces of Europe, North Africa and the*
783 *Atlantic Margins*. 159–173., <https://doi.org/10.1016/B978-0-12-809417-4.00008-2>.
- 784 Merlin Energy Resources Consortium. 2020. The Standard Stratigraphic Nomenclature of
785 Offshore Ireland: An Integrated Lithostratigraphic, Biostratigraphic and Sequence
786 Stratigraphic Framework. Project Atlas. Petroleum Affairs Division, Department of the
787 Environment, Climate and Communications, Special Publication **1/21**.
- 788 Meyer, R., van Wijk, J. & Gernigon, L. 2007. The North Atlantic Igneous Province: A review
789 of models for its formation. In: *Special Paper 430: Plates, Plumes and Planetary*
790 *Processes*. 525–552., [https://doi.org/10.1130/2007.2430\(26\)](https://doi.org/10.1130/2007.2430(26)).
- 791 Naylor, D. & Shannon, P.M. 2005. The structural framework of the Irish Atlantic Margin.
792 *Geological Society, London, Petroleum Geology Conference series*, **6**, 1009–1021,
793 <https://doi.org/10.1144/0061009>.
- 794 O'Reilly, B.M., Hauser, F., Jacob, A.W.B., Shannon, P.M., Makris, J. & Vogt, U. 1995. The
795 transition between the Erris and the Rockall basins: new evidence from wide-angle
796 seismic data. *Tectonophysics*, **241**, 143–163, [https://doi.org/10.1016/0040-](https://doi.org/10.1016/0040-1951(94)00166-7)
797 [1951\(94\)00166-7](https://doi.org/10.1016/0040-1951(94)00166-7).
- 798 O'Sullivan, C.M., Childs, C.J., Saqab, M.M., Walsh, J.J. & Shannon, P.M. 2021. The
799 influence of multiple salt layers on rift-basin development; The Slyne and Erris basins,
800 offshore NW Ireland. *Basin Research*, 1–31, <https://doi.org/10.1111/bre.12546>.
- 801 Peel, F.J., Travis, C.J. & Hossack, J.R. 1995. Genetic structural provinces and salt tectonics
802 of the Cenozoic offshore US Gulf of Mexico: A preliminary analysis. In: *Salt Tectonics:*
803 *A Global Perspective*. 153–175.
- 804 Petersen, K., Clausen, O.R. & Korstgård, J.A. 1992. Evolution of a salt-related listric growth
805 fault near the d-1 well, block 5605, Danish North Sea: displacement history and salt

- 806 kinematics. *Journal of Structural Geology*, **14**, 565–577, [https://doi.org/10.1016/0191-](https://doi.org/10.1016/0191-8141(92)90157-R)
807 8141(92)90157-R.
- 808 Quirk, D.G., Roy, S., Knott, I., Redfern, J. & Hill, L. 1999. Petroleum geology and future
809 hydrocarbon potential of the Irish Sea. *Journal of Petroleum Geology*, **22**, 243–260,
810 <https://doi.org/10.1111/j.1747-5457.1999.tb00986.x>.
- 811 Quirk, D.G. & Pilcher, R.S. 2012. Flip-flop salt tectonics. *Geological Society Special*
812 *Publication*, **363**, 245–264, <https://doi.org/10.1144/SP363.11>.
- 813 Ramos, A., Fernández, O., Muñoz, J.A. & Terrinha, P. 2017. Impact of basin structure and
814 evaporite distribution on salt tectonics in the Algarve Basin, Southwest Iberian margin.
815 *Marine and Petroleum Geology*, **88**, 961–984,
816 <https://doi.org/10.1016/j.marpetgeo.2017.09.028>.
- 817 Rowan, M.G. 1993. A systematic technique for the sequential restoration of salt structures.
818 *Tectonophysics*, **228**, 331–348, [https://doi.org/10.1016/0040-1951\(93\)90347-M](https://doi.org/10.1016/0040-1951(93)90347-M).
- 819 Rowan, M.G. & Ratliff, R.A. 2012. Cross-section restoration of salt-related deformation: Best
820 practices and potential pitfalls. *Journal of Structural Geology*, **41**, 24–37,
821 <https://doi.org/10.1016/j.jsg.2011.12.012>.
- 822 Saqab, M.M., Childs, C., Walsh, J. & Delogkos, E. 2020. Multiphase deformation history of
823 the Porcupine Basin, offshore west Ireland. *Basin Research*, 1–22,
824 <https://doi.org/10.1111/bre.12535>.
- 825 Sclater, J.G. & Christie, P.A.F. 1980. Continental stretching: An explanation of the Post-Mid-
826 Cretaceous subsidence of the central North Sea Basin. *Journal of Geophysical*
827 *Research: Solid Earth*, **85**, 3711–3739, <https://doi.org/10.1029/JB085iB07p03711>.
- 828 Shannon, P.M. 1991. The development of Irish offshore sedimentary basins. *Journal of the*
829 *Geological Society*, **148**, 181–189, <https://doi.org/10.1144/gsjgs.148.1.0181>.
- 830 Shannon, P.M. 2018. Old challenges, new developments and new plays in Irish offshore
831 exploration. *Geological Society, London, Petroleum Geology Conference series*, **8**,
832 171–185, <https://doi.org/10.1144/PGC8.12>.
- 833 Snidero, M., Carrera, N., Mencos, J., Butillé, Granado, P., Tavani, S., Lopez-Mir, B., Sàbat,
834 F. & Muñoz, J.A. 2020. Diapir kinematics in a multi-layer salt system from the eastern
835 Persian Gulf. *Marine and Petroleum Geology*, **117**, 104402,
836 <https://doi.org/10.1016/j.marpetgeo.2020.104402>.
- 837 Statoil 2004. Well 19/11-1 & 1A Final Well Report. Statoil Exploration (Ireland) Ltd., compiled
838 by Hofsøy, R., Skagen, J., Mortensen, H. & Conroy, J.
- 839 Stoker, M.S., Stewart, M.A., Shannon, P.M., Bjerager, M., Nielsen, T., Blischke, A.,
840 Hjelstuen, B.O., Gaina, C., McDermott, K. & Ólavsdóttir. 2017. An overview of the
841 Upper Palaeozoic–Mesozoic stratigraphy of the NE Atlantic region. *Geological Society,*
842 *London, Special Publications*, **447**, 11–68, <https://doi.org/10.1144/SP447.2>.
- 843 Štolfová, K. & Shannon, P.M. 2009. Permo-Triassic development from Ireland to Norway:
844 basin architecture and regional controls. *Geological Journal*, **44**, 652–676,
845 <https://doi.org/10.1002/gj.1187>.

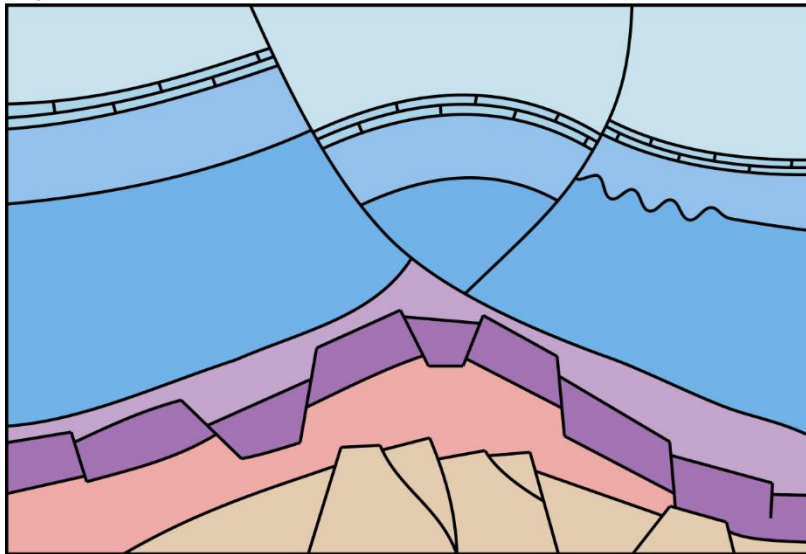
- 846 Shell 2011. Exploration Well IRE 18/20-G Wellbores 18/20-sb01 and 18/20-7 Final Well
847 Report Volume 2: Subsurface Section. Shell E&P Ireland Ltd., compiled by van
848 Koolwijk, M., Soek, H. & Stordal, T.
- 849 Stewart, S.A. & Coward, M.P. 1995. Synthesis of salt tectonics in the southern North Sea,
850 UK. *Marine and Petroleum Geology*, **12**, 457–475, [https://doi.org/10.1016/0264-](https://doi.org/10.1016/0264-8172(95)91502-G)
851 [8172\(95\)91502-G](https://doi.org/10.1016/0264-8172(95)91502-G).
- 852 Stewart, S.A., Harvey, M.J., Otto, S.C. & Weston, P.J. 1996. Influence of salt on fault
853 geometry: Examples from the UK salt basins. *Geological Society Special Publication*,
854 **100**, 175–202, <https://doi.org/10.1144/GSL.SP.1996.100.01.12>.
- 855 Tari, G., Molnar, J. and Ashton, P. 2003. Examples of salt tectonics from West Africa: A
856 comparative approach. *Geological Society Special Publication*, **207**, 85–104,
857 <https://doi.org/10.1144/GSL.SP.2003.207.5>.
- 858 Trueblood, S. & Morton, N. 1991. Comparative Sequence Stratigraphy and Structural Styles
859 of the Slyne Trough and Hebrides Basin. *Journal of the Geological Society*, **148**, 197–
860 201, <https://doi.org/10.1144/gsjgs.148.1.0197>.
- 861 Volozh, Y., Talbot, C. & Ismail-Zadeh, A. 2003. Salt structures and hydrocarbons in the
862 Pricaspian basin. *American Association of Petroleum Geologists Bulletin*, **87**, 313–334,
863 <https://doi.org/10.1306/09060200896>.
- 864 Walsh, A., Knag, G., Morris, M., Quinquis, H., Tricker, P., Bird, C. & Bower, S. 1999.
865 Petroleum geology of the Irish Rockall Trough – a frontier challenge. *Petroleum*
866 *Geology of Northwest Europe: Proceedings of the 5th Conference*, 433–444,
867 <https://doi.org/10.1144/0050433>.
- 868 Walsh, J.J. & Watterson, J. 1991. Geometric and kinematic coherence and scale effects in
869 normal fault systems. *Geological Society Special Publication*, **56**, 193–203,
870 <https://doi.org/10.1144/GSL.SP.1991.056.01.13>.
- 871 Walsh, J.J., Bailey, W.R., Childs, C., Nicol, A. & Bonson, C.G. 2003. Formation of
872 segmented normal faults: A 3-D perspective. *Journal of Structural Geology*, **25**, 1251–
873 1262, [https://doi.org/10.1016/S0191-8141\(02\)00161-X](https://doi.org/10.1016/S0191-8141(02)00161-X).
- 874 Withjack, M.O. & Callaway, S. 2000. Active normal faulting beneath a salt layer: An
875 experimental study of deformation patterns in the cover sequence. *AAPG Bulletin*, **84**,
876 627–651.
- 877 Wilson, R.C.L., Hiscott, R.N., Willis, M.G. & Gradstein, F.M. 1989. The Lusitanian Basin of
878 west-central Portugal: Mesozoic and Tertiary tectonic, stratigraphic, and subsidence
879 history. *Extensional tectonics and stratigraphy of the North Atlantic margins*, 341–361.
- 880 Ziegler, P.A. & Dèzes, P. 2006. Crustal evolution of Western and Central Europe. *Geological*
881 *Society, London, Memoirs*, **32**, 43–56, <https://doi.org/10.1144/gsl.mem.2006.032.01.03>.



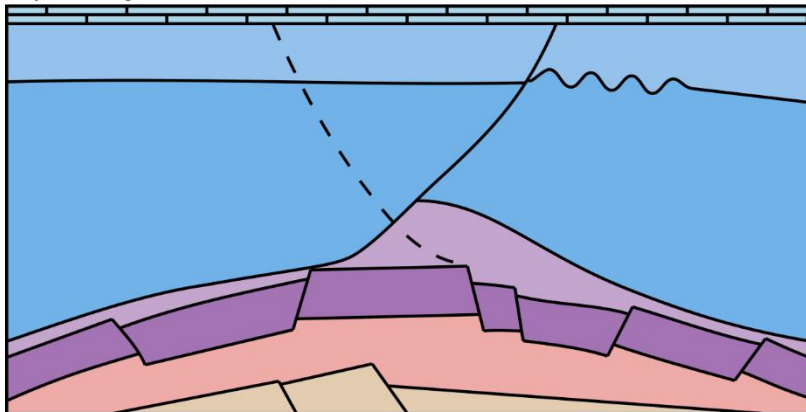
884 Figure 1: **A)** time structure map of the Lower Triassic Corrib Sandstone Formation in the
 885 Northern Slyne Sub-basin with outlines of 3D seismic volumes shown. Faults at Lower
 886 Triassic level shown with thick black polygons. **B)** Regional map showing the location of
 887 the study area and morphology of the Slyne Basin and neighbouring areas adapted
 888 from O’Sullivan et al. (2021). **C)** Regional bathymetry of the Irish Atlantic margin. **D)**
 889 Regional arbitrary seismic line and accompanying geoseismic section showcasing the
 890 structural style of the Northern Slyne Sub-basin. Note the impact of Cenozoic thermal

subsidence along the NW margin of the basin.

C) Late Jurassic



B) early Middle Jurassic



A) Early Jurassic

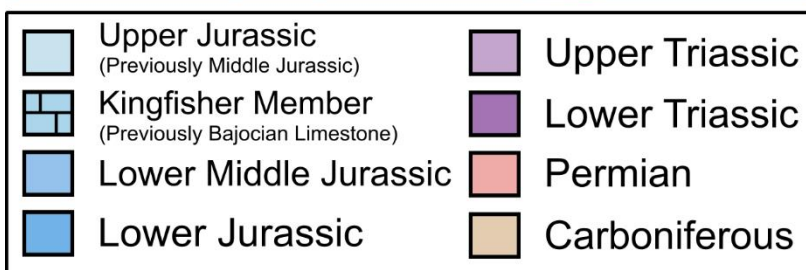
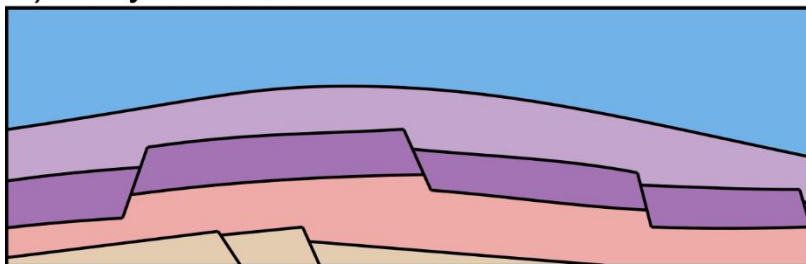
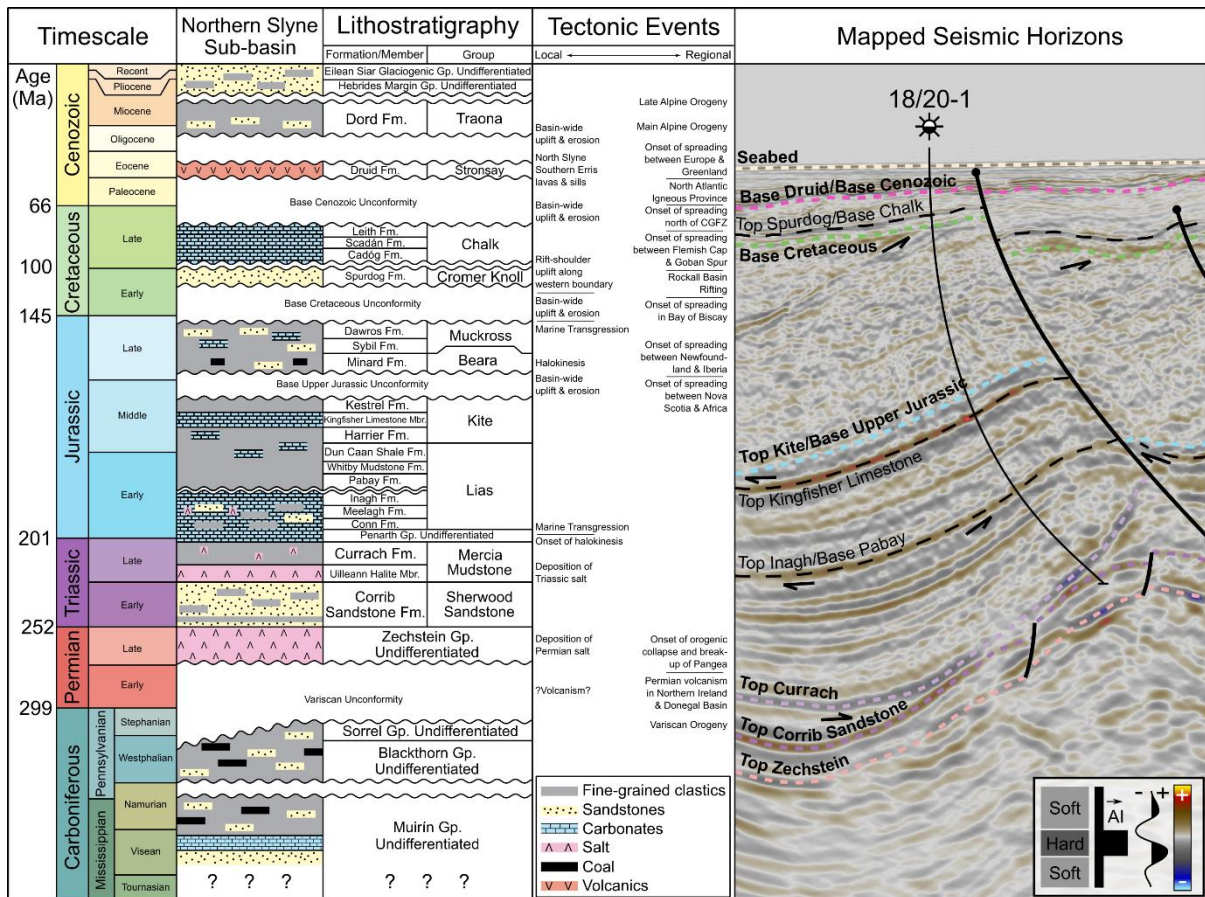


Figure 2: Previous model for the evolution of the Corrib structure, adapted from Dancer et al., 2005.



895

896 Figure 3: Simplified chronostratigraphic chart for the Northern Slyne Sub-basin showing the
 897 lithostratigraphic framework, local and regional tectonic events, and type seismic
 898 section through the Corrib gas field. Lithostratigraphic nomenclature adapted from

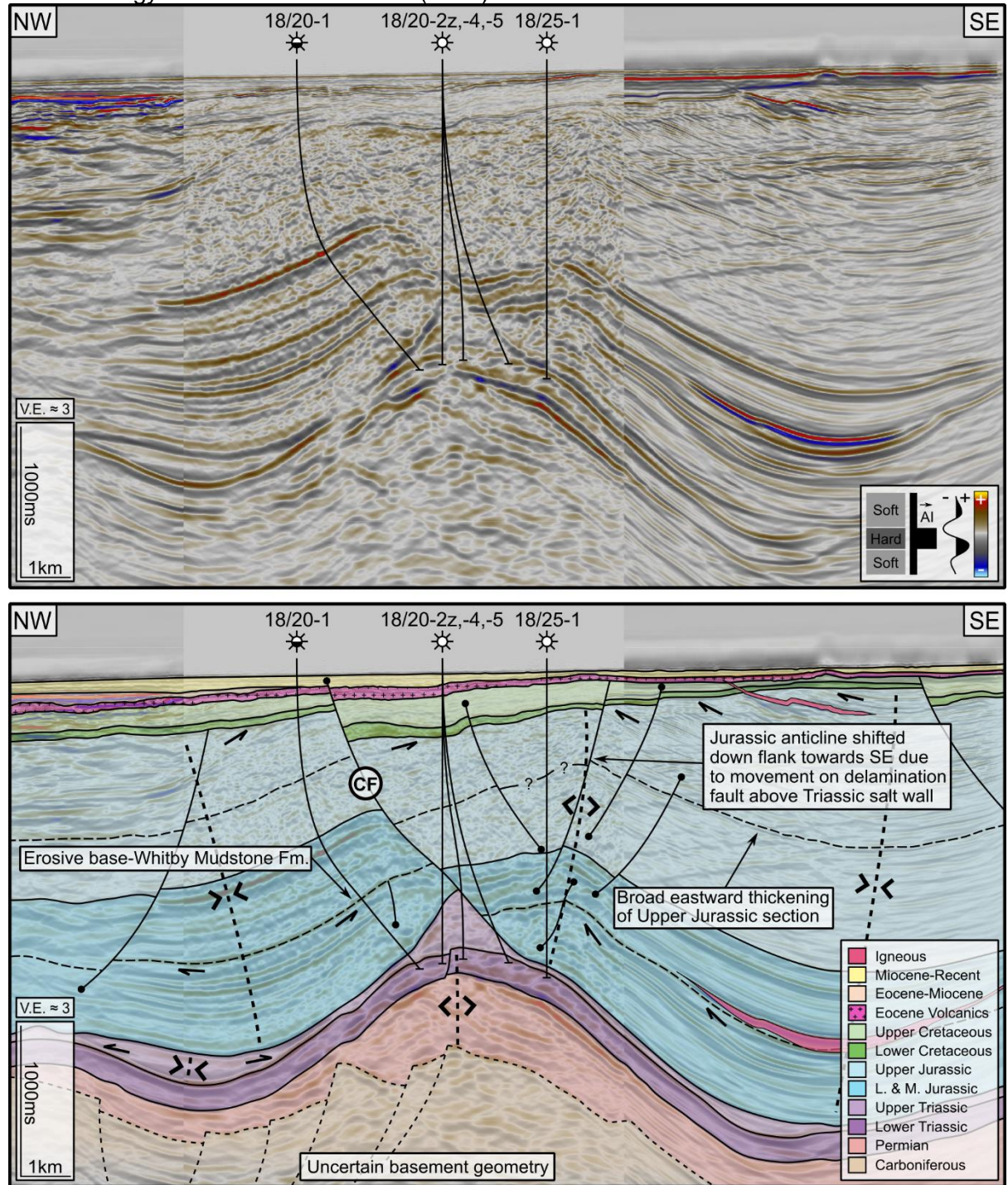
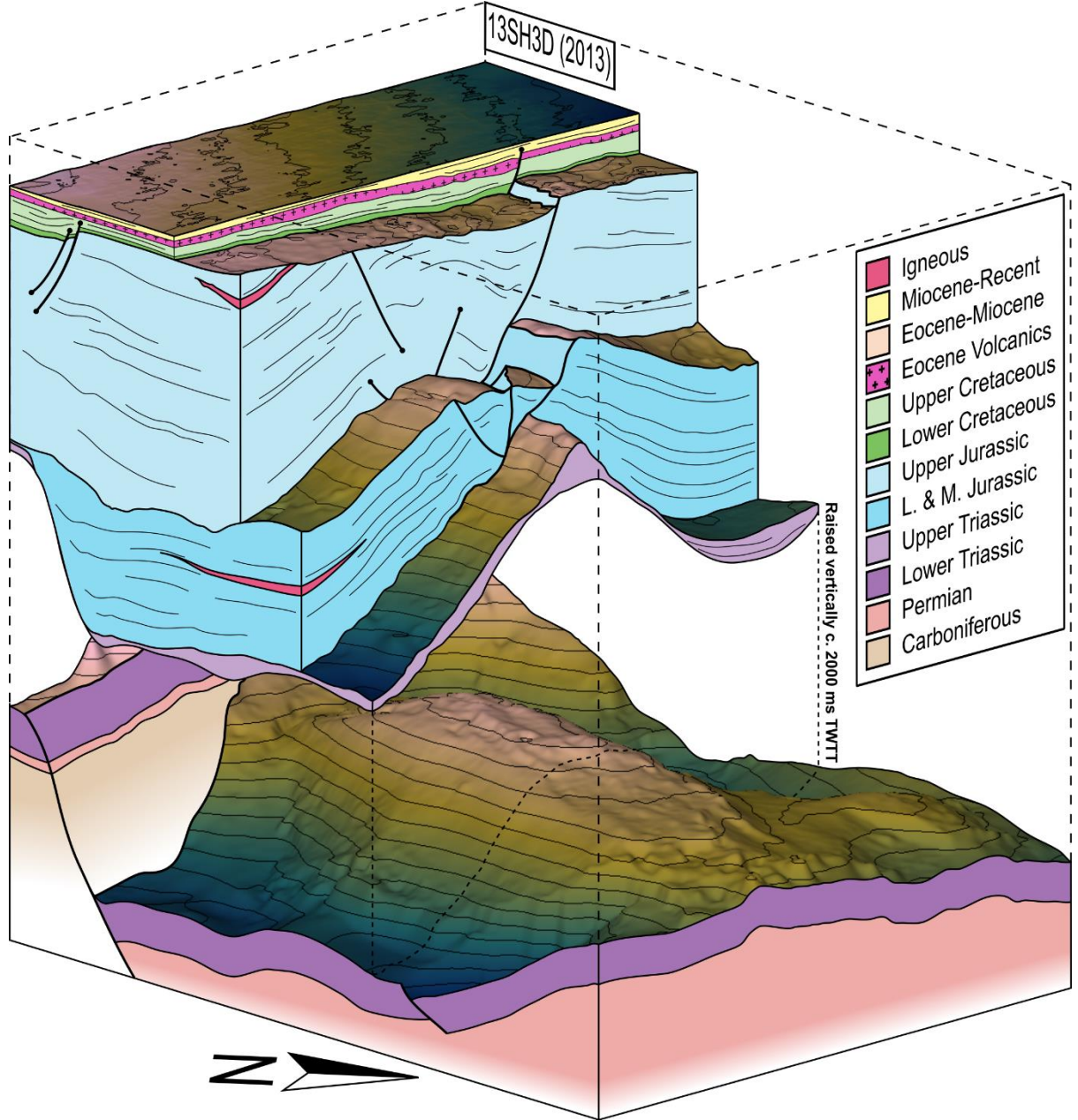


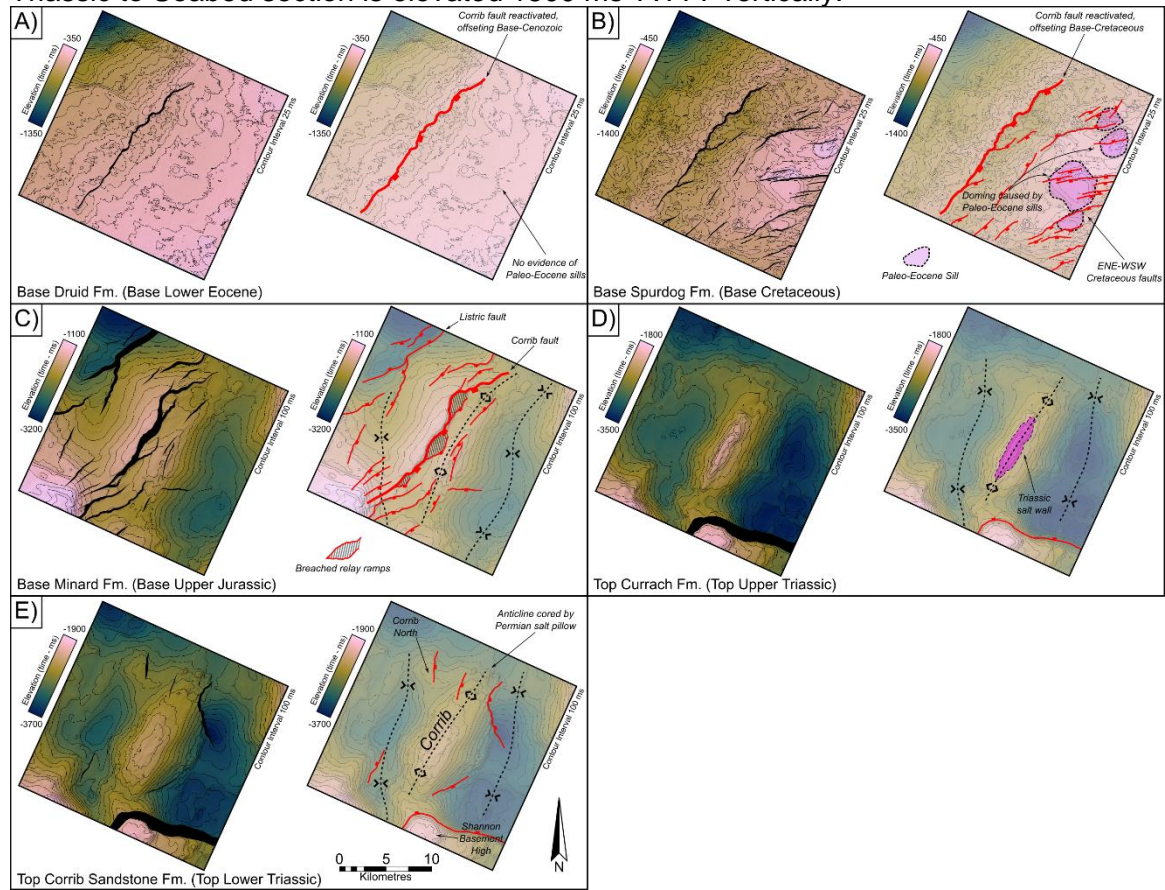
Figure 4: Composite section of the EN3D97-REPRO and 13SH3D seismic volumes and accompanying geoseismic interpretation across the Corrib gas field. See Figure 1 for



905 Figure 5: 3D block diagram illustrating the structural configuration of the Corrib gas field,
906 constructed from interpreted horizons within the 13SH3D seismic volume. The Upper

907

Triassic to Seabed section is elevated 1500 ms TWTT vertically.



908

909

Figure 6: Time structure maps in ms TWTT created from the EN3D97-REPRO seismic

910

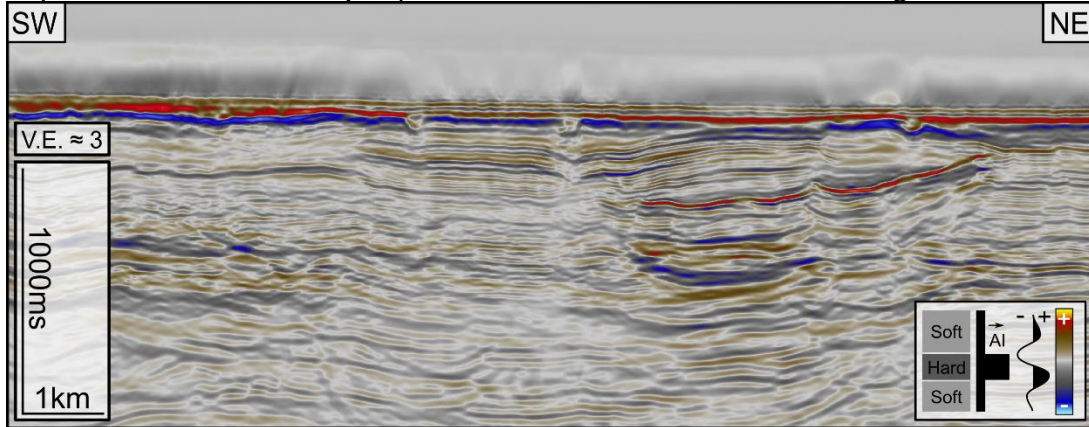
volume illustrating the structural geometries observed at different stratigraphic levels.

911

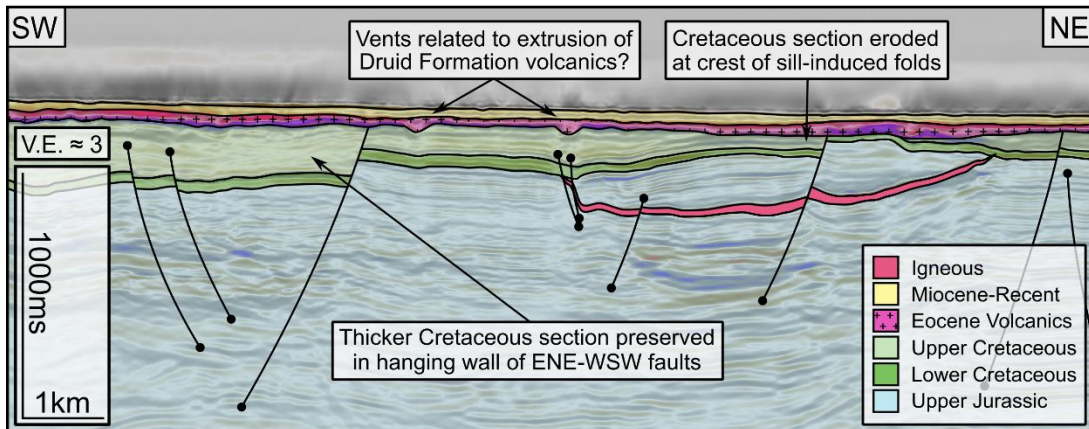
A) Base Druid Formation. **B)** Base Spurdog Formation. **C)** Base Minard Formation. **D)**

912

Top Currach Formation. **E)** Top Corrib Sandstone Formation. See Figure 1 for location.



913

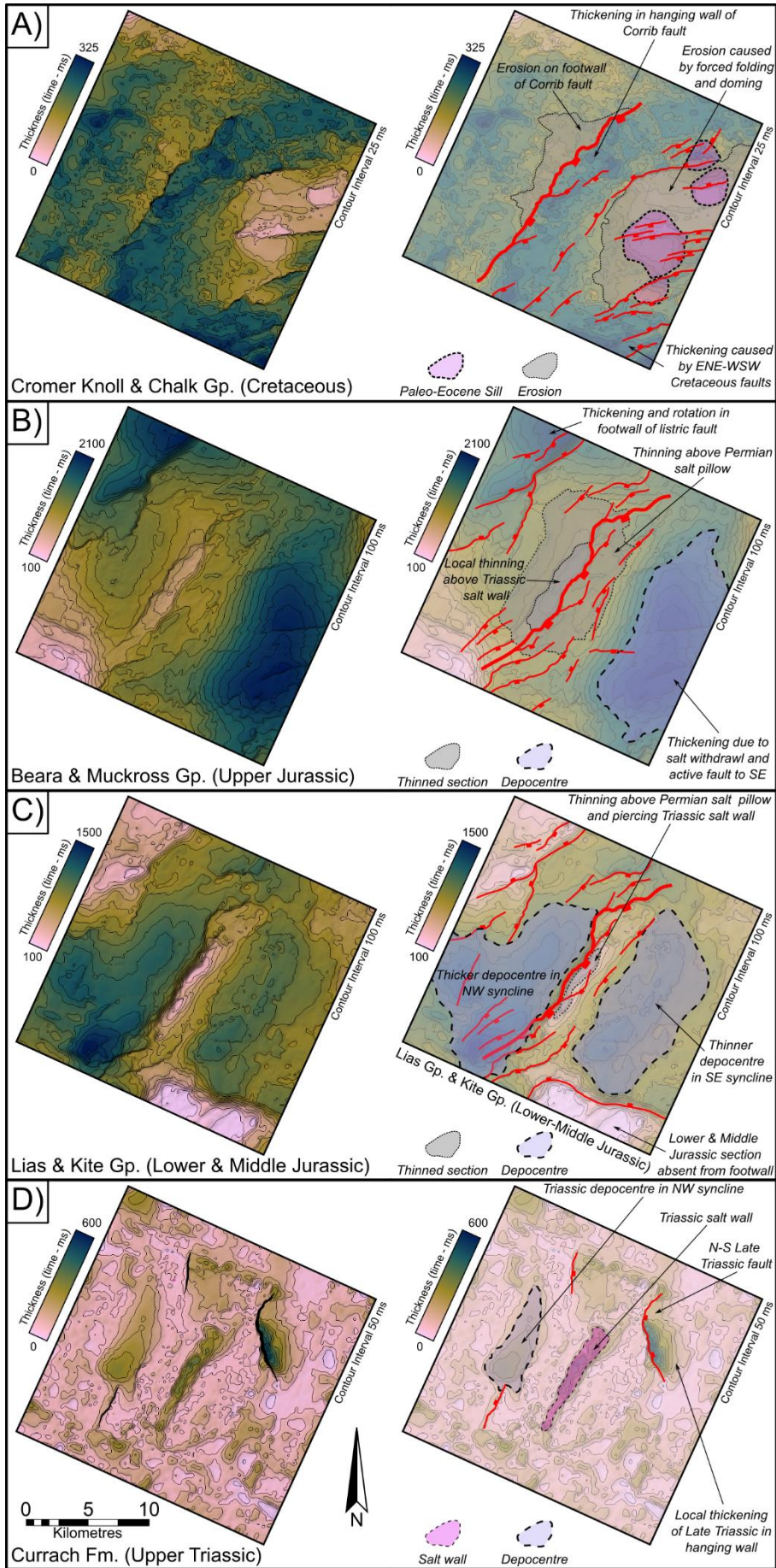


914

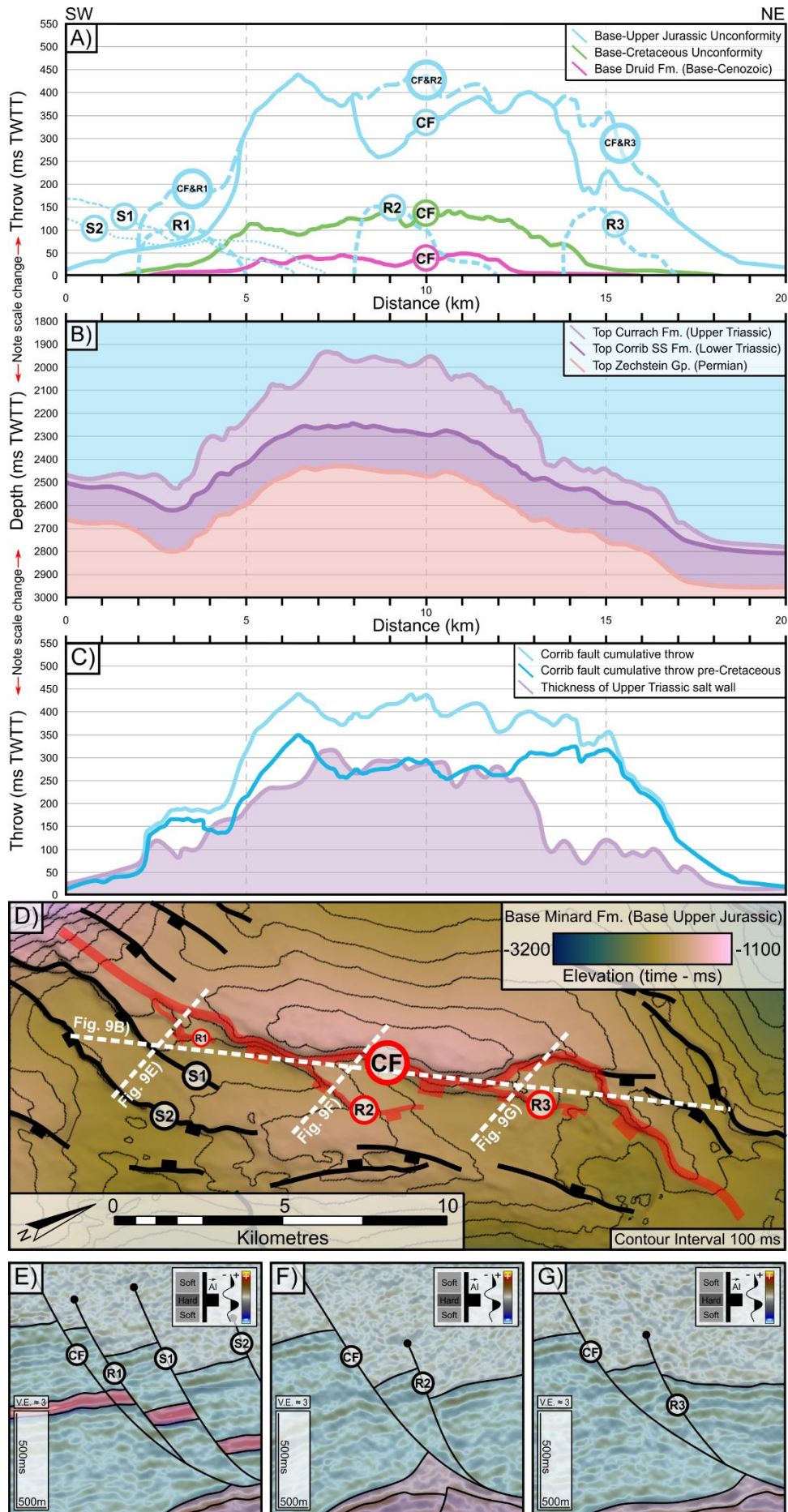
Figure 7: Seismic section and accompanying geoseismic interpretation of the shallow

915

geology to the SE of the Corrib gas field, highlighting the impact of Cenozoic igneous

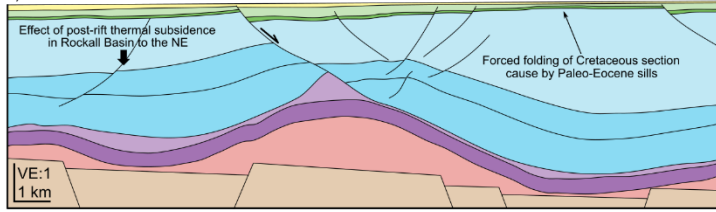


918 Figure 8: Time thickness (isochron) maps in ms TWTT created from horizons presented in
919 Figure 5. **A)** Cromer Knoll & Chalk groups. **B)** Beara and Muckross groups. **C)** Lias and

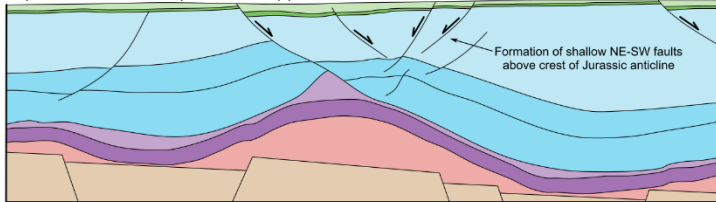


922 Figure 9: **A)** Throw-distance (T-x) plot displaying the along-strike throw of the Corrib fault
923 system for prominent syn-rift and post-rift horizons. **Abbreviations:** CF – Corrib Fault;
924 R1-3 – Hanging wall splays; S1-2 – Additional faults; CF&RX – cumulative throw of
925 Corrib fault and hanging wall splay. **B)** Simplified cross-section through the time-
926 structure maps of the Top Currach and Corrib Sandstone formations and Zechstein
927 Group. For cross-section location see Figure 7D). **C)** Throw-distance (T-x) plot
928 displaying the along-strike throw of the Corrib fault for the Base Upper Jurassic
929 Unconformity alongside the backstripped pre-Cretaceous throw, and the thickness of
930 the Upper Triassic salt wall. **D)** Time structure map of the Base Minard Formation
931 adjacent to the listric fault system, highlighting the fault planes displayed in Figure 7A).

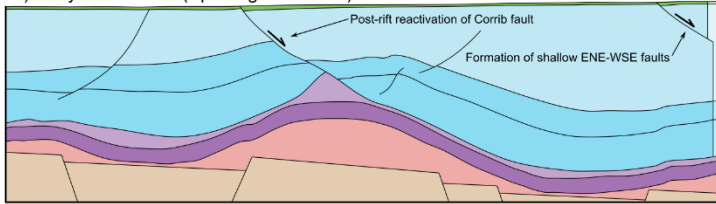
I) Cenozoic to Present



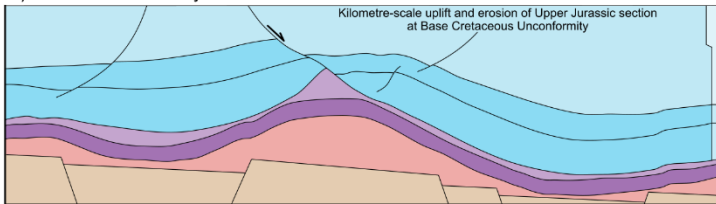
H) Late Cretaceous (Chalk Group)



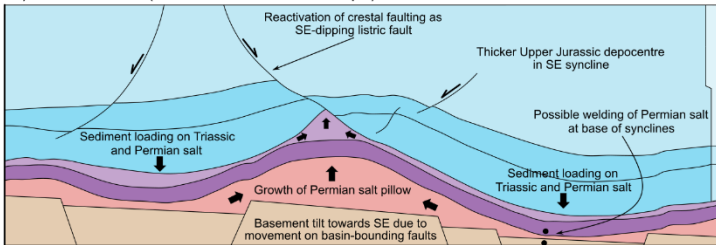
G) Early Cretaceous (Spurdog Formation)



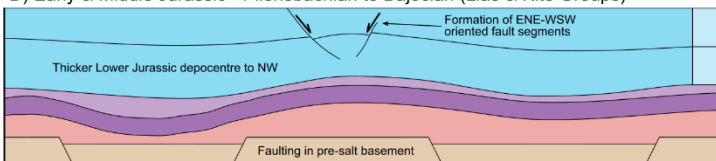
F) End Jurassic & Early Cretaceous



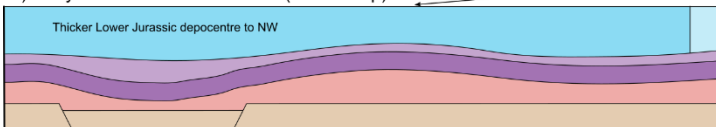
E) Late Jurassic (Beara & Muckross Groups)



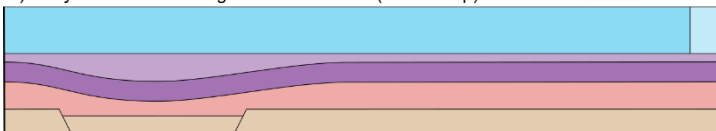
D) Early & Middle Jurassic - Pliensbachian to Bajocian (Lias & Kite Groups)



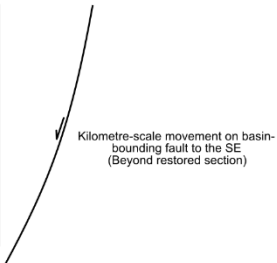
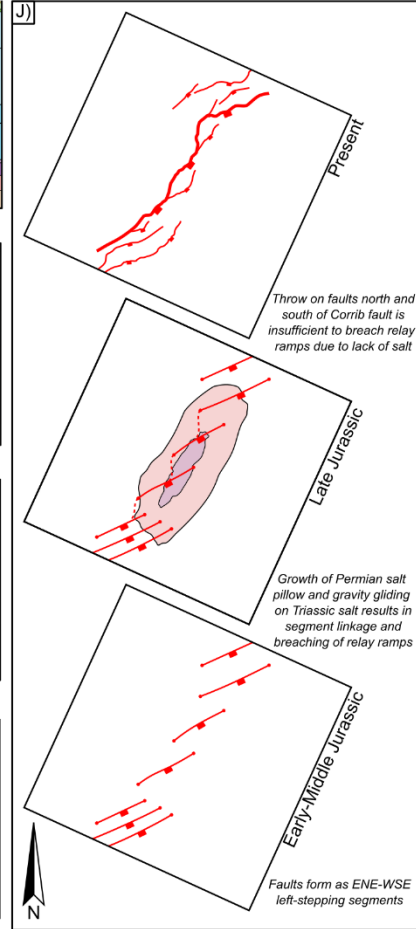
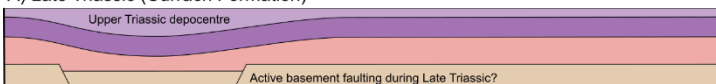
C) Early Jurassic - Pliensbachian (Lias Group)



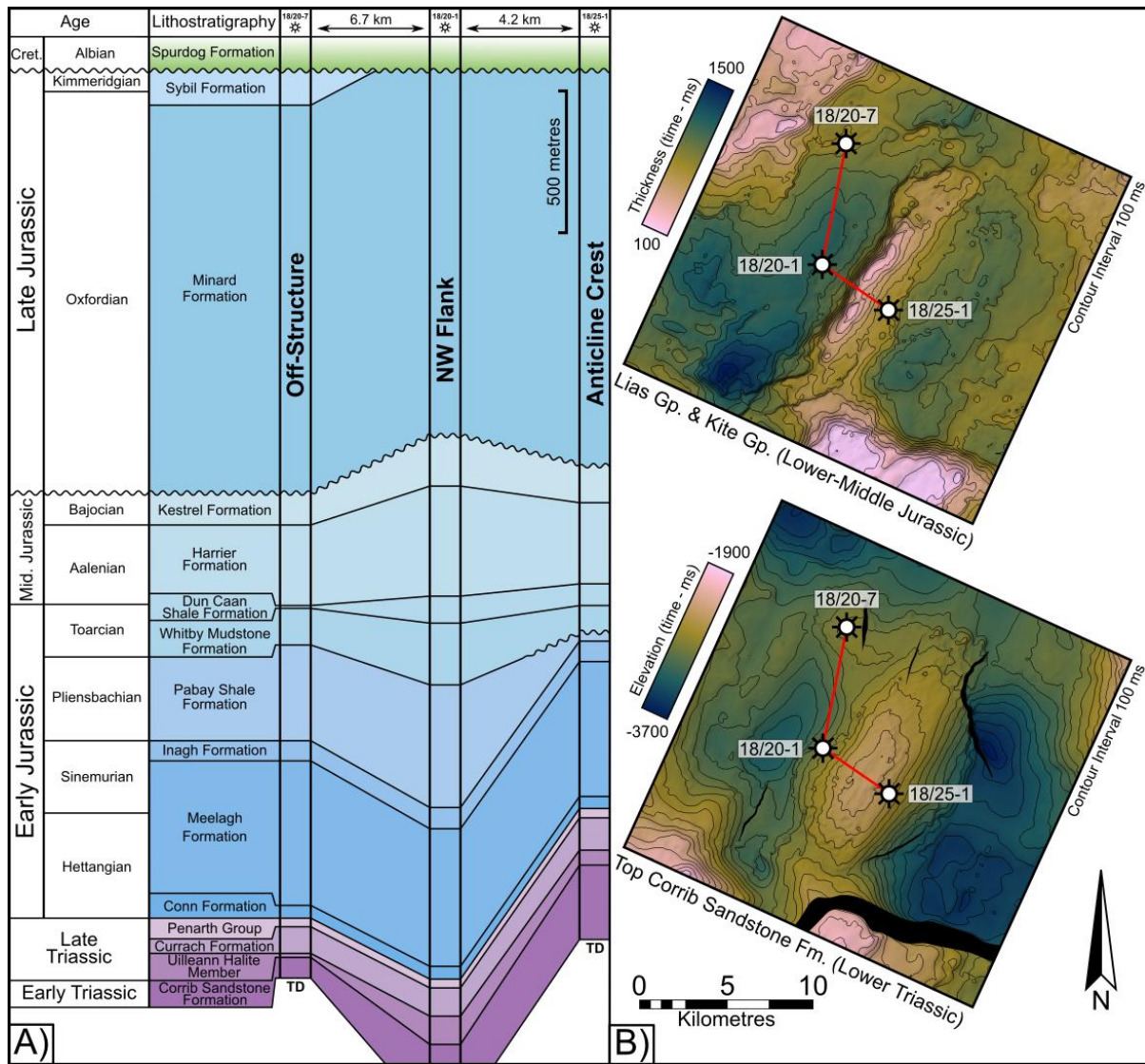
B) Early Jurassic - Hettangian to Sinemurian (Lias Group)



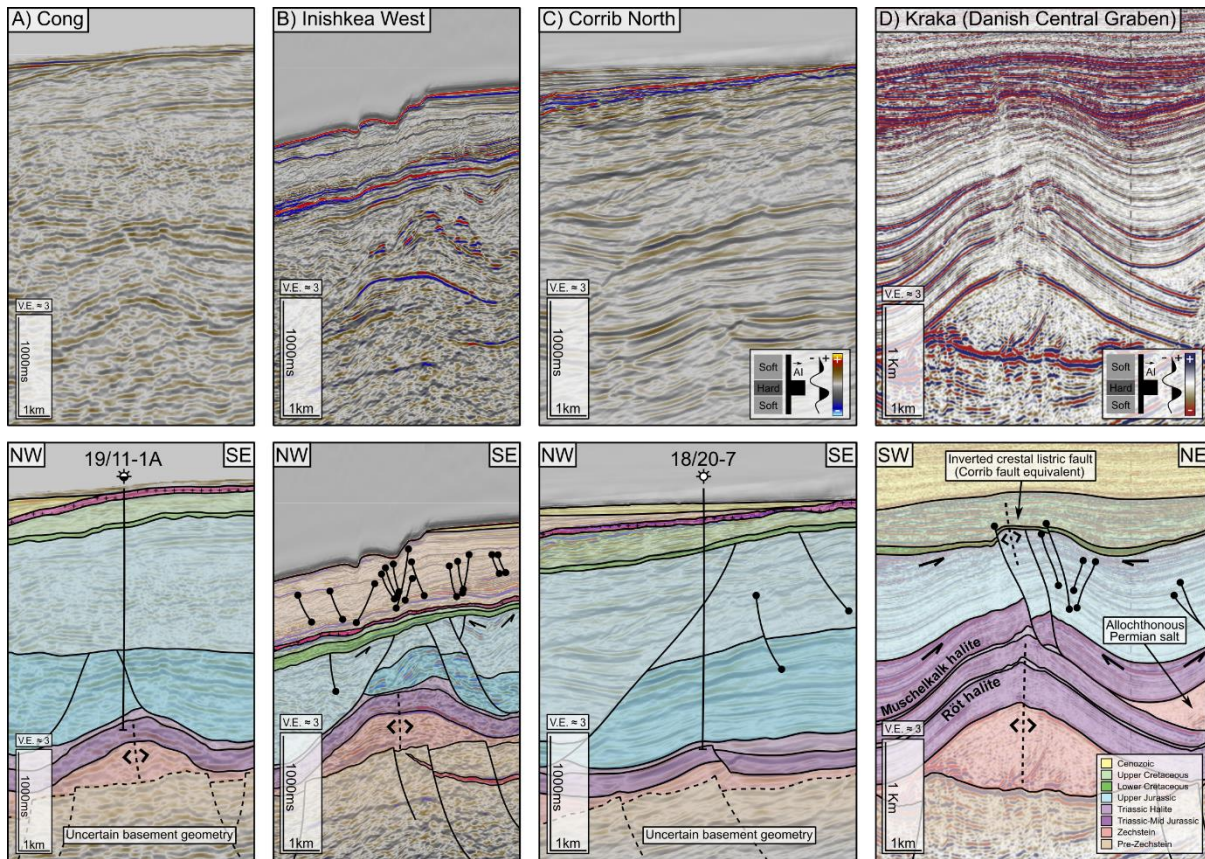
A) Late Triassic (Currach Formation)



934 Figure 10: Sequential structural restoration of the interpreted seismic section presented in
 935 Figure 3 with no vertical exaggeration. Due to uncertainty in the actual geometry of the
 936 sub-salt basement in the Northern Slyne Sub-basin, a schematic basement is included
 937 to suggest potential drivers for halokinesis based on interpretation of basement
 938 structures elsewhere in the Slyne Basin (e.g. O'Sullivan et al., 2021). Inset: schematic
 939 evolution of the fault system in the supra-salt Jurassic section.



940
 941 **Figure 11: A)** Well correlation through the three wells which penetrate a complete Jurassic
 942 section within the EN3D97-REPRO seismic volume. The Base-Cretaceous
 943 Unconformity is the datum. The 18/20-7 well is representative of the Jurassic section
 944 off-structure, while the 18/20-1 is representative of the Early Jurassic depocenter on the
 945 NW flank. The 18/25-1 well showcases the Early-Middle Jurassic crest of the salt-cored
 946 fold, before the listric fault downthrows this crest onto the SE flank of the structure
 947 during the Late Jurassic. Notice the isopachous nature of the Conn, Meelagh and Inagh
 948 formations. **B)** Time thickness (isochron) map of the Lias and Kite groups and a time
 949 structure map of the Corrib Sandstone Formation, both in ms TWTT, showing the
 950 location of the well correlation.



951

952 Figure 12: Seismic sections and accompanying geoseismic interpretations showing
 953 analogues to the Corrib gas field in the Slyne Basin and other areas. **A-C)** Corrib
 954 analogues in the Slyne Basin. See Figure 1 for seismic line locations. **D)** Corrib
 955 analogue in the Danish Central Graben. Seismic data and interpretation adapted from
 956 Hansen et al., 2021.

957 Table 1: Values used to depth convert seismic sections for structural restoration. Values
 958 derived from well-based velocity data.

Stratigraphic interval	V_0	k
Water column (surface to seabed)	1500	N/A
Cenozoic	1510	N/A
Cretaceous	2756	N/A
Upper Jurassic	2483	0.50
Lower & Middle Jurassic	3200	0.40
Upper Triassic	4400	0.20
Lower Triassic	4800	0.15

959